Cell Reports

Article

ADAR1 restricts ZBP1-mediated immune response and PANoptosis to promote tumorigenesis

Graphical abstract

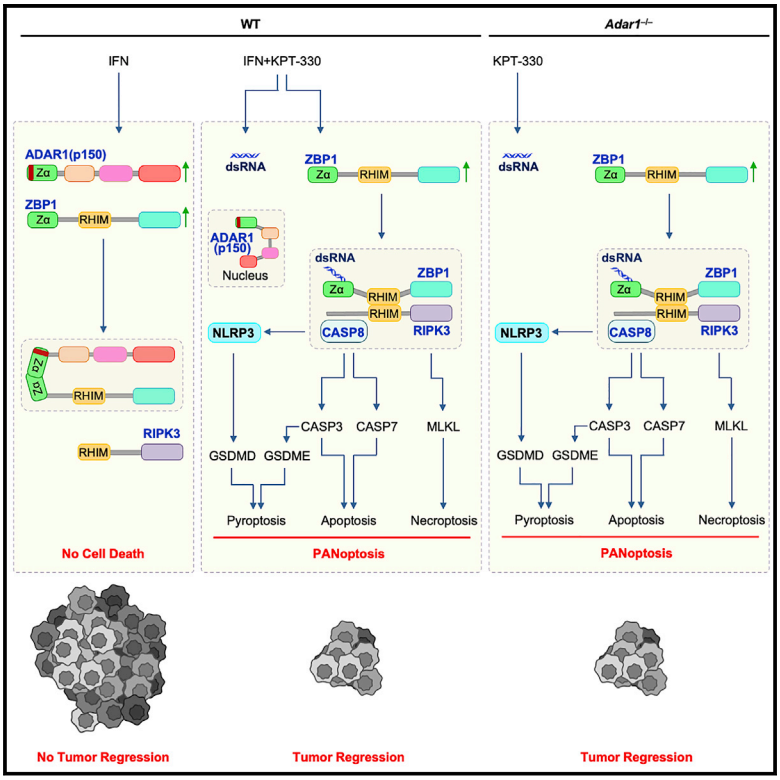

Highlights

- Combining IFNs with NEIs induces ZBP1-mediated inflammatory cell death, PANoptosis
- ADAR1 negatively regulates the ZBP1-mediated PANoptosis
- Blocking ADAR1 activity unleashes ZBP1-mediated PANoptosis to inhibit tumorigenesis
- In mice, IFN-γ + KPT-330 dramatically regresses tumors in a ZBP1-dependent manner

Authors

Rajendra Karki, Balamurugan Sundaram, Bhesh Raj Sharma, ..., Geoffrey Neale, Peter Vogel, Thirumala-Devi Kanneganti

Correspondence

thirumala-devi.kanneganti@stjude.org

In brief

Karki et al. identify a critical role for ADAR1 in regulating ZBP1-mediated inflammatory cell death, PANoptosis. Treating with IFNs, which upregulate ADAR1 and ZBP1, and nuclear export inhibitors, which sequester ADAR1 in the nucleus, induces robust cell death that inhibits tumorigenesis *in vivo*, suggesting a therapeutic strategy.

Karki et al., 2021, Cell Reports *37*, 109858
October 19, 2021
https://doi.org/10.1016/j.celrep.2021.109858

CellPress

Cell Reports

CellPress
OPEN ACCESS

Article

ADAR1 restricts ZBP1-mediated immune response and PANoptosis to promote tumorigenesis

Rajendra Karki,[1] Balamurugan Sundaram,[1] Bhesh Raj Sharma,[1] SangJoon Lee,[1] R.K. Subbarao Malireddi,[1] Lam Nhat Nguyen,[1] Shelbi Christgen,[1] Min Zheng,[1] Yaqiu Wang,[1] Parimal Samir,[1] Geoffrey Neale,[2] Peter Vogel,[3] and Thirumala-Devi Kanneganti[1,4,*]

[1]Department of Immunology, St. Jude Children's Research Hospital, Memphis, TN 38105, USA
[2]Hartwell Center for Bioinformatics & Biotechnology, St. Jude Children's Research Hospital, Memphis, TN 38105, USA
[3]Animal Resources Center and Veterinary Pathology Core, St. Jude Children's Research Hospital, Memphis, TN 38105, USA
[4]Lead contact
*Correspondence: thirumala-devi.kanneganti@stjude.org
https://doi.org/10.1016/j.celrep.2021.109858

SUMMARY

Cell death provides host defense and maintains homeostasis. Zα-containing molecules are essential for these processes. Z-DNA binding protein 1 (ZBP1) activates inflammatory cell death, PANoptosis, whereas adenosine deaminase acting on RNA 1 (ADAR1) serves as an RNA editor to maintain homeostasis. Here, we identify and characterize ADAR1's interaction with ZBP1, defining its role in cell death regulation and tumorigenesis. Combining interferons (IFNs) and nuclear export inhibitors (NEIs) activates ZBP1-dependent PANoptosis. ADAR1 suppresses this PANoptosis by interacting with the Zα2 domain of ZBP1 to limit ZBP1 and RIPK3 interactions. *Adar1*$^{fl/fl}$*LysM*^{cre} mice are resistant to development of colorectal cancer and melanoma, but deletion of the ZBP1 Zα2 domain restores tumorigenesis in these mice. In addition, treating wild-type mice with IFN-γ and the NEI KPT-330 regresses melanoma in a ZBP1-dependent manner. Our findings suggest that ADAR1 suppresses ZBP1-mediated PANoptosis, promoting tumorigenesis. Defining the functions of ADAR1 and ZBP1 in cell death is fundamental to informing therapeutic strategies for cancer and other diseases.

INTRODUCTION

Nucleic acids, particularly double-stranded RNA (dsRNA) from pathogens, are sensed by cytosolic RNA sensors to produce type I interferons (IFNs), which provide host defense against invading microbes (Yoneyama et al., 2004). However, the sensors can also recognize some endogenous RNAs, such as short interspersed nuclear elements and endogenous retroelements (EREs), leading to sustained and profound IFN production in the absence of infection (Ahmad et al., 2018; Jiao et al., 2020; Kim et al., 2004; Neeman et al., 2006; Wang et al., 2020). To avoid this pathological overactivation of the immune system, host RNAs undergo a post-transcriptional RNA base modification catalyzed by adenosine deaminase acting on RNA 1 (ADAR1), preventing the sensing of endogenous dsRNA (Nishikura, 2010). ADAR1 is critical for development and survival (Hartner et al., 2004, 2009; Liddicoat et al., 2015; Wang et al., 2000). Mutations in ADAR1 and the subsequent sustained type I IFN response have been associated with several autoimmune and autoinflammatory disorders, such as Aicardi-Goutieres syndrome (AGS), systemic lupus erythematosus, and bilateral striatal necrosis (Tang et al., 2018). In addition, although the underlying mechanisms remain unclear, recent studies have suggested an association between ADAR1 and tumorigenesis (Fumagalli et al., 2015; Han et al., 2015; Liu et al., 2019; Paz-Yaacov et al., 2015; Tassinari et al., 2021).

There are two major isoforms of ADAR1, p150 and p110, with ADAR1-p150 being the IFN-inducible form and shuttling between the nucleus and cytoplasm (Eckmann et al., 2001; George and Samuel, 1999a, 1999b). Moreover, ADAR1-p150 contains a Z-alpha (Zα) domain (Schwartz et al., 1999). Besides ADAR1, the only other mammalian protein that contains Zα domains is Z-DNA binding protein 1 (ZBP1) (Schwartz et al., 2001), which recognizes viral and endogenous Z-RNAs (Devos et al., 2020; Jiao et al., 2020; Kesavardhana et al., 2020; Kuriakose et al., 2016; Wang et al., 2020; Zhang et al., 2020). The Zα domains of ZBP1 recognize Z-RNAs in macrophages to activate the NLRP3 inflammasome and PANoptosis, an inflammatory programmed cell death pathway regulated by the PANoptosome complex with key features of pyroptosis, apoptosis, and/or necroptosis that cannot be accounted for by any of these three pathways alone (Christgen et al., 2020; Gurung et al., 2014; Karki et al., 2021; Kuriakose et al., 2016; Zheng et al., 2020). Multiple PANoptosomes have been described to date, and ZBP1 has been implicated in the formation of both the ZBP1-PANoptosome (Christgen et al., 2020; Zheng et al., 2020) and the AIM2-PANoptosome (Lee et al., 2021). Although both ADAR1-p150 and ZBP1 contain Zα domains and are IFN inducible, whether ADAR1 functions similarly to ZBP1 in cell death processes is unclear.

Within its Zα domain, ADAR1-p150 also contains a nuclear export signal (NES) (Poulsen et al., 2001). Chromosomal maintenance 1 (CRM1), also known as exportin 1 (XPO1), mediates the

export of ADAR1-p150 to the cytoplasm using its NES. Mutation of the NES or treatment with nuclear export inhibitors (NEIs) specific to XPO1 causes nuclear accumulation of ADAR1-p150 and cell death (Poulsen et al., 2001). Whether this is similar to the PANoptotic cell death induced by ZBP1 is unknown. Similar to the detrimental effects of increased ADAR1 expression, XPO1 overexpression correlates with poor prognosis in various cancers (Taylor et al., 2019). Treatments targeting XPO1, such as selective NEIs, are beneficial in cancer treatment (Azizian and Li, 2020). NEIs such as leptomycin B (LMB) or Selinexor (KPT-330) have anti-tumor efficacy in several preclinical models of solid tumor and hematological malignancies (Gravina et al., 2014). Moreover, KPT-330 has recently received US Food and Drug Administration (FDA) approval for use in patients with relapsed/refractory multiple myeloma (Chari et al., 2019; Theodoropoulos et al., 2020).

Here, we identified and characterized the relationship between two Zα domain-containing proteins, ADAR1 and ZBP1, in cell death. Using ADAR1-deficient macrophages, we found that ADAR1 competes with RIPK3 for binding to ZBP1 to inhibit cell death; when ADAR1 is lost or sequestered in the nucleus by NEI treatment, ZBP1 can function in the cytoplasm without hindrance to drive inflammatory cell death, PANoptosis. Furthermore, melanoma growth and colorectal cancer tumorigenesis were suppressed in *Adar1*$^{fl/fl}$*LysM*^{cre} mice, while deficiency of ZBP1 or the Zα2 domain of ZBP1 in these mice restored the tumor growth. Additionally, treating mice with the combination of IFN-γ, to upregulate IFN-stimulated genes (ISGs) including ZBP1 and ADAR1, and the NEI KPT-330, to sequester ADAR1 to the nucleus, significantly regressed melanoma in a ZBP1- and Zα2 domain-dependent manner. These findings highlight the important roles of the ADAR1-ZBP1 interaction in cell death and cancer.

RESULTS

IFN signaling potentiates the cell death induced by nuclear transport inhibitors

The nucleo-cytoplasmic transport of proteins and RNAs plays a crucial role in maintaining normal cellular functions and homeostasis (Eckmann et al., 2001). One of the major eukaryotic nuclear exporters that mediates the transport of proteins with an NES is XPO1. Selective targeting of XPO1-mediated nuclear export by NEIs has anti-tumor effects (Chari et al., 2019; Theodoropoulos et al., 2020), which may be due to the ability of NEIs to induce cancer cell death (Mutka et al., 2009). Therefore, molecularly defining the cell death pathways induced by NEIs is critical to understand the molecular mechanisms by which NEIs inhibit tumorigenesis.

To determine whether NEIs can induce cell death, we treated bone-marrow-derived macrophages (BMDMs) with the NEIs KPT-330 or LMB. Treatment with either KPT-330 or LMB for 24 h induced a low level of cell death in BMDMs (Figures 1A–1C). Certain cytokines, such as TNF or IL-1β and IFN signaling, potentiate cell death in a context-dependent manner (Karki et al., 2021; Man et al., 2016; Sarhan et al., 2019; Shen et al., 2017; Yang et al., 2020). Additionally, cytokine-based therapies have been used historically to treat cancer in both preclinical and clinical studies (Aricò et al., 2019). Therefore, we evaluated the effect of combining NEIs with cytokine treatment on cell death. Treatment with IFN-β or IFN-γ in combination with KPT-330 or LMB increased the incidence of cell death compared with treatment with KPT-330 or LMB alone (Figures 1A–1C, S1A, and S1B), while treatment with other cytokines, including TNF, IL-1β, or IL-6, in combination with KPT-330 or LMB, failed to increase the incidence of cell death (Figures S1A and S1B). This suggests that IFN signaling potentiates the cell death induced by NEIs.

To investigate whether NEIs can induce pyroptotic inflammatory cell death, we monitored the cleavage of the pyroptosis effector gasdermin D (GSDMD). Treatment with NEIs led to production of a small amount of the active GSDMD P30 fragment (Figure 1D). GSDMD can be processed to release this P30 fragment by caspase-1 or caspase-11 (He et al., 2015; Kayagaki et al., 2015; Shi et al., 2015). Consistent with the amount of GSDMD P30 produced, there was minimal cleavage of caspase-1 and caspase-11 in response to NEIs alone (Figure 1D). Another member of the gasdermin family, GSDME, can also induce pyroptosis under specific conditions (Wang et al., 2017). We observed that BMDMs treated with KPT-330 or LMB also displayed minimal cleavage of GSDME (Figure 1D), demonstrating that NEIs induced a low level of pyroptotic effector activation in BMDMs. In addition to pyroptosis, we also found that KPT-330 or LMB induced the activation of apoptotic effectors in BMDMs, as evidenced by the cleavage of apoptotic caspase-8, -3, and -7 (Figure 1E). Furthermore, recent studies have shown that activation of caspase-3 and -7 can inactivate GSDMD by processing it to produce a P20 fragment (Chen et al., 2019; Taabazuing et al., 2017), which we also observed (Figure 1D). Next, we examined whether the NEIs induced necroptosis. Cells stimulated with KPT-330 or LMB showed a low level of phosphorylation of MLKL (Figure 1F), suggesting that the activation of necroptotic effectors is occurring.

We next evaluated the cell death mechanisms induced by the combination of NEIs with IFN. In line with the incidence of cell death, treatment with IFN-β or IFN-γ potentiated KPT-330- or LMB-induced cleavage of caspase-1 and GSDME (pyroptosis); cleavage of caspase-8, -3, and -7 (apoptosis); and phosphorylation of MLKL (necroptosis) (Figures 1D–1F). Collectively, these data suggest that combining IFNs with NEIs sensitizes the cells to undergo inflammasome activation and cell death involving the components of pyroptosis, apoptosis, and necroptosis, indicating that PANoptosis is occurring.

ZBP1 engages RIPK3 signaling to activate the NLRP3 inflammasome and PANoptosis induced by NEIs

Innate immune sensors play critical roles in activating the inflammasome and driving cell death (Man et al., 2017). Because combining IFNs and NEIs induced caspase-1 cleavage, we first investigated whether the cytosolic sensors that are known to assemble inflammasomes activated caspase-1 and induced cell death under these conditions. The minimal caspase-1 cleavage induced by NEIs alone or robust caspase-1 cleavage induced by the combination of IFN-β and NEIs was impaired in *Nlrp3*$^{-/-}$ and *Asc*$^{-/-}$ BMDMs, but not in *Nlrc4*$^{-/-}$, *Aim2*$^{-/-}$, *Mefv*$^{-/-}$, or *Casp11*$^{-/-}$ BMDMs (Figure S1C), indicating that the combination of IFNs with NEIs activates the NLRP3 inflammasome. Despite the defective caspase-1 cleavage, cell death was not impaired

CellPress
OPEN ACCESS

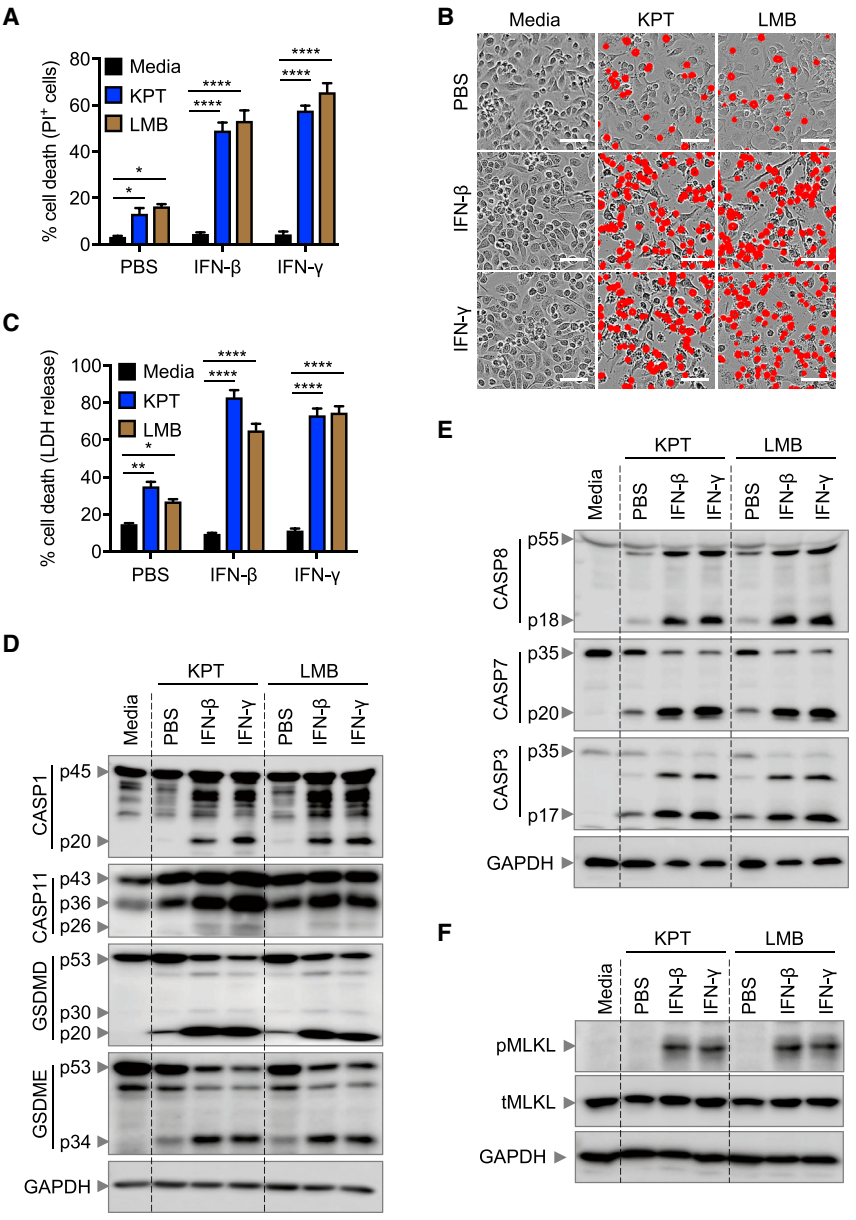

Figure 1. Interferons potentiate the cell death induced by nuclear export inhibitors

(A–C) Quantification of cell death by propidium iodide (PI) staining (A), representative images of cell death (B), and quantification of cell death by LDH release in wild-type (WT) BMDMs treated with KPT-330 (KPT) or leptomycin B (LMB) for 24 h in the presence or absence of IFN-β or IFN-γ (C).

(D–F) Immunoblot analysis of (D) pro- (p45) and activated (p20) caspase-1 (CASP1), pro- (p43) and cleaved caspase-11 (CASP11; p36 and p26), pro- (p53), activated (p30), and inactivated (p20) gasdermin D (GSDMD), and pro- (p53) and activated (p34) gasdermin E (GSDME); (E) pro- (p55) and cleaved caspase-8 (CASP8; p18), pro- (p35) and cleaved caspase-7 (CASP7; p20), pro- (p35) and cleaved caspase-3 (CASP3; p17); and (F) phosphorylated MLKL (pMLKL) and total MLKL (tMLKL) in WT BMDMs treated with KPT or LMB for 24 h in the presence or absence of IFN-β or IFN-γ. GAPDH was used as the internal control. Data are representative of at least three independent experiments. Scale bars, 50 μm. *$p < 0.05$; **$p < 0.01$; ****$p < 0.0001$. Analysis was performed using the two-way ANOVA. Data are shown as mean ± SEM (A and C; n = 4 in each treatment group).

in *Nlrp3*$^{-/-}$ and *Asc*$^{-/-}$ BMDMs (Figure S1D), suggesting that other molecules are involved in regulating cell death. Next, we screened other innate immune sensors that are known to regulate inflammasome activation and cell death in various contexts (Man et al., 2017). We found that BMDMs lacking ZBP1 had reduced cell death compared with wild-type (WT) BMDMs after IFN-β and NEI treatment (Figures 2A–2C and S2A). Consistent with this protection, *Zbp1*$^{-/-}$ BMDMs showed reduced activation of pyroptotic, apoptotic, and necroptotic molecules (Figures 2D–2F), suggesting that ZBP1 is required for IFN- and NEI-induced NLRP3 inflammasome activation and PANoptosis.

Sensing of viral or endogenous Z-RNA by the Zα domains of ZBP1 triggers NLRP3 inflammasome activation, inflammatory cell death, and perinatal lethality in mice, indicating that the Zα domains are crucial to regulate the ZBP1-mediated immune responses (Devos et al., 2020; Jiao et al., 2020; Kesavardhana et al., 2020). Therefore, we investigated the role of the Zα2 domain of ZBP1 in driving the inflammasome activation and cell death induced by IFN and NEIs. Similar to *Zbp1*$^{-/-}$ BMDMs, cells lacking the Zα2 domain of ZBP1 showed reduced cell death compared with that of WT BMDMs after treatment with IFN-β and KPT-330 or IFN-β and LMB (Figures 2A–2C). Consistent with the reduced cell death, *Zbp1*$^{\Delta Z\alpha 2}$ BMDMs showed impaired activation of pyroptotic, apoptotic, and necroptotic effectors (Figures 2D–2F). Together, these results indicated that the Zα2 domain of ZBP1 is required for IFN- and NEI-induced activation of the NLRP3 inflammasome and PANoptosis.

ZBP1 activation leads to its interaction with RIPK3 and recruitment of caspase-8 and caspase-6 to form a cell death signaling scaffold, termed the ZBP1-PANoptosome, that drives NLRP3 inflammasome activation and cell death (Kesavardhana et al., 2020; Kuriakose et al., 2016; Rebsamen et al., 2009; Zheng et al., 2020). We therefore assessed whether RIPK3 and caspase-8 had any role in the NEI-induced cell death pathways. Similar to *Zbp1*$^{-/-}$ or *Zbp1*$^{\Delta Z\alpha 2}$ BMDMs, cells lacking RIPK3 showed reduced cell death and activation of pyroptotic, apoptotic, and necroptotic molecules compared with that of WT BMDMs after IFN-β and KPT-330 or IFN-β and LMB treatment (Figures S2B–S2E). We did not observe significant differences in the extent of cell death between *Ripk3*$^{-/-}$ and *Ripk3*$^{-/-}$*Casp8*$^{-/-}$ BMDMs (Figures S2B–S2E), indicating that the phenotype observed in

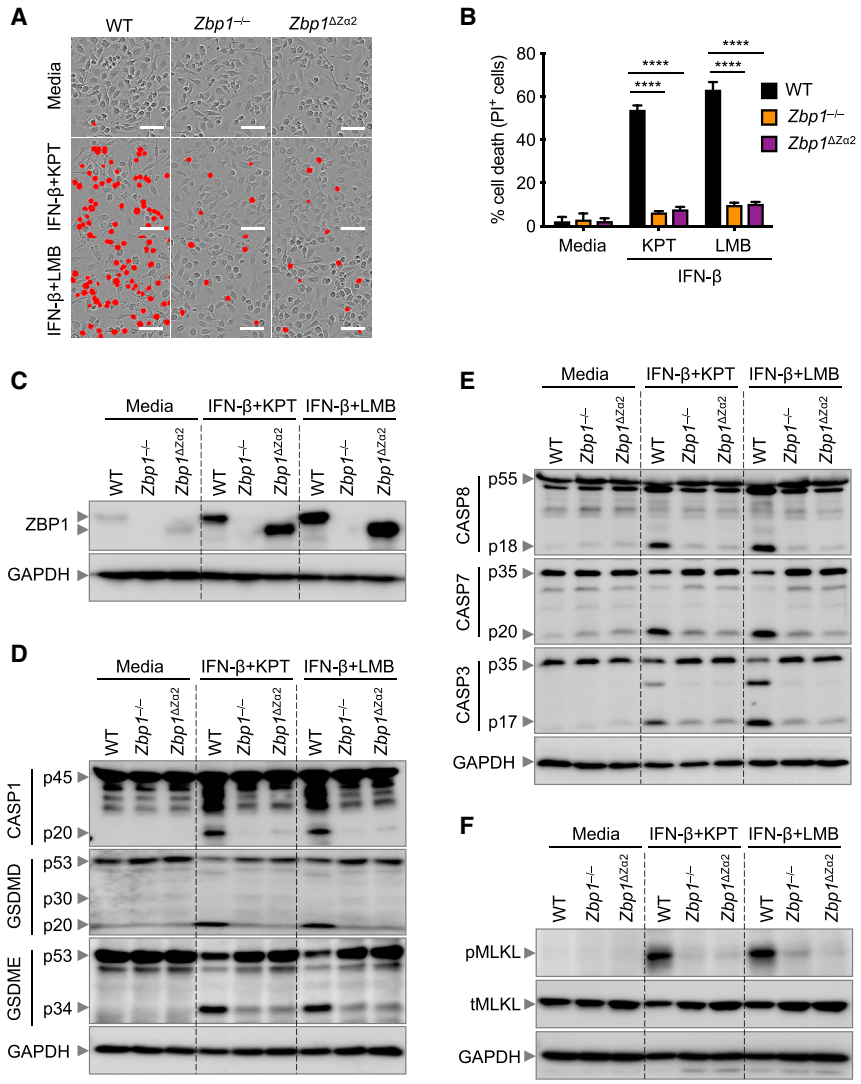

Figure 2. ZBP1 triggers inflammasome activation and cell death in response to the combination of IFNs and nuclear export inhibitors

(A and B) Representative images of cell death (A) and quantification of cell death (B) in WT, *Zbp1*$^{-/-}$, and *Zbp1*$^{\Delta Z\alpha 2}$ BMDMs treated with KPT-330 (KPT) or leptomycin B (LMB) for 24 h in the presence of IFN-β. (C–F) Immunoblot analysis of (C) ZBP1; (D) pro- (p45) and activated (p20) caspase-1 (CASP1), pro- (p53), activated (p30), and inactivated (p20) GSDMD, and pro- (p53) and activated (p34) gasdermin E (GSDME); (E) pro- (p55) and cleaved caspase-8 (CASP8; p18), pro- (p35) and cleaved caspase-7 (CASP7; p20), pro- (p35) and cleaved caspase-3 (CASP3; p17); and (F) phosphorylated MLKL (pMLKL) and total MLKL (tMLKL) in WT, *Zbp1*$^{-/-}$, and *Zbp1*$^{\Delta Z\alpha 2}$ BMDMs treated with KPT or LMB for 24 h in the presence of IFN-β. GAPDH was used as the internal control. Data are representative of at least three independent experiments. Scale bars, 50 μm. ****$p < 0.0001$. Analysis was performed using the two-way ANOVA. Data are shown as mean ± SEM (B; n = 4 for each genotype).

Ripk3$^{-/-}$*Casp8*$^{-/-}$ BMDMs is largely attributed to the RIPK3 deficiency, because caspase-8 is downstream of RIPK3.

To determine the contribution of other critical cell death molecules to the inflammatory cell death induced by IFNs and NEIs, we examined the role of the pyroptosis initiators (CASP1 and CASP11), pyroptosis executioners (GSDMD and GSDME), apoptosis executioners (CASP3 and CASP7), and necroptosis executioner (MLKL) in the cell death. The extent of cell death in *Casp1*$^{-/-}$, *Casp11*$^{-/-}$, *Gsdmd*$^{-/-}$, *Gsdme*$^{-/-}$, *Casp3*$^{-/-}$, *Casp7*$^{-/-}$, and *Mlkl*$^{-/-}$ BMDMs was similar to that in WT BMDMs following treatment with NEIs in the presence or absence of IFN-β priming (Figures S3A and S3B), which could be due to redundancies among the executioners of different cell death pathways. Additionally, *Gsdmd*$^{-/-}$*Gsdme*$^{-/-}$ cells showed reduced cell death compared with WT, *Gsdmd*$^{-/-}$, or *Gsdme*$^{-/-}$ cells. However, combined deletion of GSDMD, GSDME, and MLKL resulted in a similar level of protection as that of cells lacking both GSDMD and GSDME (Figures S3A and S3B), suggesting that GSDMD and GSDME collectively potentiate the inflammatory cell death in response to NEIs with or without IFN priming.

Altogether, these data suggest that the Zα2 domain of ZBP1 is required to activate RIPK3 signaling to induce activation of the NLRP3 inflammasome and the execution of cell death that depends on GSDMD and GSDME collectively in response to the combination of IFNs and NEIs.

ADAR1 suppresses ZBP1-mediated NLRP3 inflammasome activation and PANoptosis

In addition to ZBP1, the only other mammalian protein that contains a Zα domain is the ADAR1-p150 splice isoform (Schwartz et al., 1999). However, the relationship between these two molecules is not known. Given that both ADAR1-p150 and ZBP1 contain Zα domains, it is tempting to speculate that ADAR1 can act similarly to ZBP1 and promote inflammasome activation and PANoptosis. In addition to its Zα domain, ADAR1-p150 also contains an NES; inhibition of the nuclear export by XPO1-specific NEIs such as KPT-330 or LMB induces nuclear accumulation of ADAR1 (Poulsen et al., 2001).

Because ADAR1-deficient mice are embryonically lethal (Hartner et al., 2004, 2009; Liddicoat et al., 2015; Wang et al., 2000), we derived BMDMs from mice lacking ADAR1 in myeloid cells (*Adar1*$^{fl/fl}$*LysM*^{cre}, referred to as *Adar1*$^{-/-}$ BMDMs in the text) to investigate the role of ADAR1 in NEI-mediated inflammasome activation and PANoptosis. We observed increased cell death induced by the combination of IFN-β and KPT-330 or IFN-β and LMB in the cells lacking ADAR1 compared with those of WT and *Zbp1*$^{-/-}$ cells (Figures 3A and 3B). Moreover, analysis of real-time cell death showed that ADAR1-deficient BMDMs

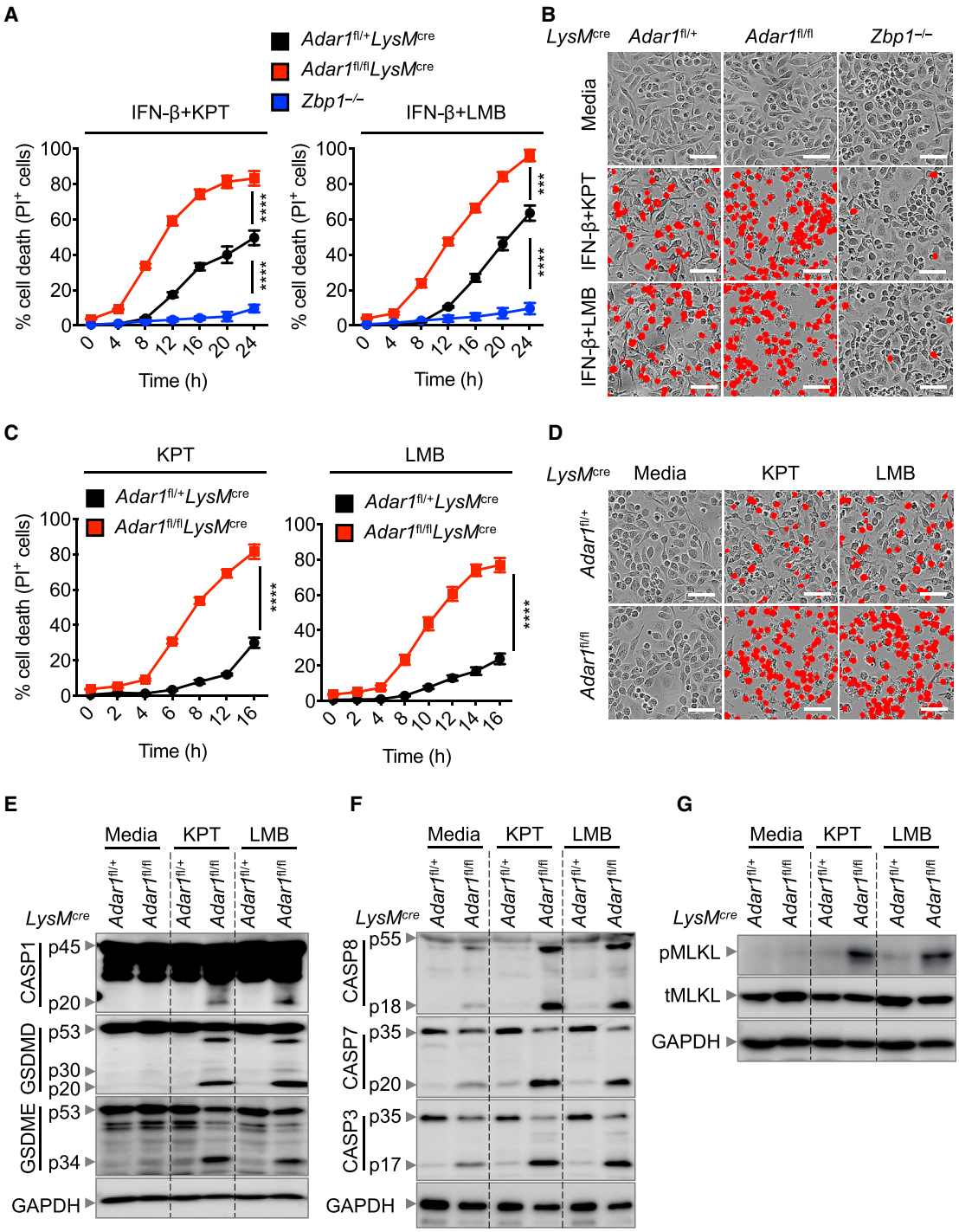

Figure 3. ADAR1 deficiency leads to accelerated cell death in response to nuclear export inhibitors

(A and B) Real-time analysis of cell death (A) and representative images of cell death (B) in *Adar1*$^{fl/+}$*LysM*^{cre}, *Adar1*$^{fl/fl}$*LysM*^{cre}, and *Zbp1*$^{-/-}$ BMDMs treated with KPT-330 (KPT) or leptomycin B (LMB) in the presence of IFN-β for 24 h.

(C and D) Real-time analysis of cell death (C) and representative images of cell death (D) in *Adar1*$^{fl/+}$*LysM*^{cre} and *Adar1*$^{fl/fl}$*LysM*^{cre} BMDMs treated with KPT or LMB alone for 16 h.

(E–G) Immunoblot analysis of (E) pro- (p45) and activated (p20) caspase-1 (CASP1), pro- (p53), activated (p30), and inactivated (p20) GSDMD, and pro- (p53) and activated (p34) gasdermin E (GSDME); (F) pro- (p55) and cleaved caspase-8 (CASP8; p18), pro- (p35) and cleaved caspase-7 (CASP7; p20), pro- (p35) and cleaved caspase-3 (CASP3; p17); and (G) phosphorylated MLKL (pMLKL) and total MLKL (tMLKL) in *Adar1*$^{fl/+}$*LysM*^{cre} and *Adar1*$^{fl/fl}$*LysM*^{cre} BMDMs treated with KPT or LMB for 12 h. GAPDH was used as the internal control.

Data are representative of at least three independent experiments. Scale bars, 50 μm. ***p < 0.001, ****p < 0.0001. Analysis was performed using two-way ANOVA. Data are shown as mean ± SEM (A and C; n = 4 for each genotype).

had accelerated cell death compared with WT and *Zbp1*$^{-/-}$ BMDMs (Figure 3A).

Despite the fact that both ADAR1-p150 and ZBP1 are IFN inducible and contain Zα domains (Kuriakose et al., 2018; Patterson and Samuel, 1995; Schwartz et al., 1999), these molecules showed contrasting phenotypes in terms of cell death, with loss of ZBP1 inhibiting cell death and loss of ADAR1 enhancing cell death (Figures 2, 3A, and 3B). To understand how ADAR1 deficiency contributes to enhanced cell death, we performed a microarray analysis to identify differentially regulated ISGs in WT and ADAR1-deficient BMDMs under basal condition. Consistent with previous findings (Barrett et al., 2013; Liddicoat et al., 2015), ADAR1-deficient BMDMs showed increased expression of ISGs (Figure S4A). Furthermore, analysis of a publicly available dataset identified increased expression of ISGs in ADAR1-deficient fibroblasts as well (Figure S4B). We also observed that *Zbp1* was one of the most highly upregulated ISGs in ADAR1-deficient BMDMs and fibroblasts (Figures S4A and S4B). We further validated the increased expression of ZBP1 together with other ISGs in *Adar1*$^{-/-}$ BMDMs using RT-PCR (Figure S4C; Table S1). Increased expression of ZBP1 in ADAR1-deficient BMDMs was further confirmed by western blot analysis and immunofluorescence (Figures S4D and S4E). Moreover, we observed increased phosphorylation of IRF3 and STAT1 and expression of STAT1 in *Adar1*$^{-/-}$ BMDMs (Figure S4D). All these findings suggest that deficiency of ADAR1 leads to increased ZBP1 expression.

Because ADAR1-deficient BMDMs have high ZBP1 expression basally (Figure S4), these cells could potentially be prone to NEI-induced cell death even without IFN treatment. We evaluated this possibility and found increased cell death in *Adar1*$^{-/-}$ BMDMs upon treatment with KPT-330 or LMB alone (Figures 3C and 3D). Notably, *Adar1*$^{-/-}$ BMDMs had increased cleavage of caspase-1 and activation of the pyroptotic molecule GSDME; apoptotic caspases (caspase-8, -3, and -7); and the necroptotic molecule MLKL after treatment with KPT-330 or LMB alone (Figures 3E–3G), suggesting that ADAR1 suppresses NLRP3 inflammasome activation and PANoptosis induced by NEIs.

Next, we treated WT and *Adar1*$^{-/-}$ BMDMs with an anti-IFNAR1 (IFN α/β receptor subunit 1) neutralizing antibody to evaluate the effect of IFN signaling in cell death induced by IFN and NEIs and NEIs alone. Anti-IFNAR1 antibody treatment suppressed IFN signaling and ZBP1 expression induced by IFN-β and cell death induced by the combination of IFN-β and NEIs in WT BMDMs (Figures S5A–S5C). However, *Adar1*$^{-/-}$ BMDMs underwent robust cell death induced by NEIs alone even after treatment with anti-IFNAR1 neutralizing antibody (Figures S5D and S5E). Athough anti-IFNAR1 antibody treatment inhibited IFN signaling induced by IFN-β, it did not suppress the ZBP1 expression in *Adar1*$^{-/-}$ BMDMs (Figure S5F), which likely explains the failure of the anti-IFNAR1 neutralizing antibody to inhibit cell death in *Adar1*$^{-/-}$ BMDMs. The minimal effect of the anti-IFNAR1 antibody in *Adar1*$^{-/-}$ BMDMs could be due to sustained levels of ZBP1 expression as a result of constitutive IFN signaling. These findings are consistent with previous observations in the setting of SETDB1 deficiency, in which anti-IFNAR1 neutralizing antibody inhibits IFN-β-induced ZBP1 expression in WT organoids but fails to inhibit ZBP1 expression and cell death in *Setdb1* null organoids (Wang et al., 2020). Thereafter, we generated cells lacking both ADAR1 and ZBP1 to further confirm that increased ZBP1 expression contributes to the accelerated inflammasome activation and cell death observed in the absence of ADAR1. BMDMs deficient in both ADAR1 and ZBP1 showed similar cell death to that of WT cells in response to KPT-330 or LMB (Figures 4A and 4B). Furthermore, NLRP3 inflammasome activation and the activation of pyroptotic, apoptotic, and necroptotic effectors were inhibited upon deletion of ZBP1 in *Adar1*$^{-/-}$ BMDMs treated with NEIs (Figures 4C–4E).

Overall, these results show that loss of ADAR1, similar to IFN treatment, leads to increased expression of ZBP1, which triggers accelerated inflammasome activation and PANoptosis induced by NEIs.

IFNs promote the production of EREs by NEIs to activate ZBP1

Despite having upregulated ZBP1 expression basally, *Adar1*$^{-/-}$ BMDMs still require treatment with NEIs to drive inflammatory cell death. We therefore hypothesized that KPT-330 or LMB would induce the release of triggers that activate ZBP1. Previous studies have suggested that ZBP1 senses genomic RNA from influenza A virus (IAV) through its Zα domains to trigger cell death (Kuriakose et al., 2016; Zhang et al., 2020). Considering there was no viral infection in *Adar1*$^{-/-}$ BMDMs, we investigated whether de-repressed endogenous dsRNA in the presence of NEIs could function as a trigger to prime ZBP1 and induce cell death. We observed an increase in the amount of dsRNA present in *Adar1*$^{-/-}$ BMDMs upon treatment with KPT-330 or LMB (Figures 5A and 5B). Furthermore, dsRNA from EREs have been shown to bind the Zα domain of ZBP1 to induce inflammatory cell death (Jiao et al., 2020; Wang et al., 2020). To test whether ERE-derived dsRNA could be induced by KPT-330 or LMB treatment, we examined the expression of mouse early transposon ([ETn]/*MuS-D*), long interspersed element 1 (*Line1*), murine endogenous retrovirus-like (*MuERV-L*), and intracisternal A-particle (*IAP*) in *Adar1*$^{-/-}$ cells. Treatment of *Adar1*$^{-/-}$ BMDMs with KPT-330 or LMB increased the expression of these EREs (Figure 5C; Table S1).

In contrast with *Adar1*$^{-/-}$ cells, WT BMDMs required the combination of IFNs with NEIs to induce robust amounts of cell death (Figures 1 and 3). Therefore, we sought to examine the levels of dsRNA and EREs in KPT-330- or LMB-treated WT BMDMs with or without IFN-β priming. Treatment of WT cells with KPT-330 or LMB alone increased the levels of dsRNA compared with media-treated WT cells (Figure 5D). However, the combination of IFN-β and KPT-330 or IFN-β and LMB more robustly increased dsRNA compared with PBS-, KPT-330-, or LMB-treated WT cells (Figures 5D and 5E). Moreover, the expression of EREs, such as *Mus-D*, *Line1*, and *MuERV-L*, was upregulated in cells treated with KPT-330 or LMB alone and more robustly increased in cells treated with the combination of IFN-β and KPT-330 or IFN-β and LMB (Figure 5F). Altogether, these data suggest that IFN priming in WT cells potentiates the ability of NEIs to increase the levels of endogenous dsRNA, which can be subsequently sensed by ZBP1 to mediate inflammatory cell death.

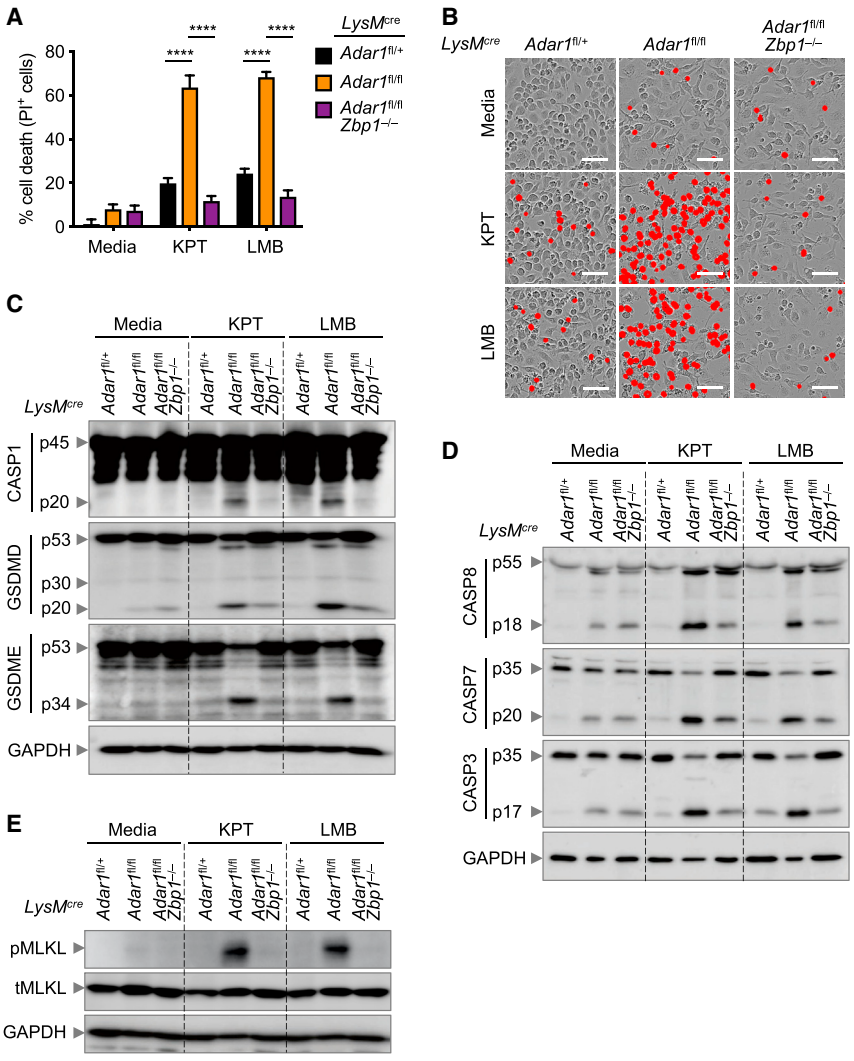

Figure 4. Deletion of ZBP1 rescues nuclear export inhibitor-induced inflammasome activation and cell death in ADAR1-deficient cells

(A and B) Quantification of cell death (A) and representative images of cell death (B) in *Adar1*$^{fl/+}$*LysM*^{cre}, *Adar1*$^{fl/fl}$*LysM*^{cre}, and *Adar1*$^{fl/fl}$*LysM*^{cre}*Zbp1*$^{-/-}$ BMDMs treated with KPT-330 (KPT) or leptomycin B (LMB) for 16 h.

(C–E) Immunoblot analysis of (C) pro- (p45) and activated (p20) caspase-1 (CASP1), pro- (p53), activated (p30), and inactivated (p20) gasdermin D (GSDMD), and pro- (p53) and activated (p34) gasdermin E (GSDME); (D) pro- (p55) and cleaved caspase-8 (CASP8; p18), pro- (p35) and cleaved caspase-7 (CASP7; p20), pro- (p35) and cleaved caspase-3 (CASP3; p17); and (E) phosphorylated MLKL (pMLKL) and total MLKL (tMLKL) in *Adar1*$^{fl/+}$*LysM*^{cre}, *Adar1*$^{fl/fl}$*LysM*^{cre}, and *Adar1*$^{fl/fl}$*LysM*^{cre}*Zbp1*$^{-/-}$ BMDMs treated with KPT or LMB for 12 h. GAPDH was used as the internal control.

Data are representative of at least three independent experiments. Scale bars, 50 μm. ****p < 0.0001. Analysis was performed using two-way ANOVA. Data are shown as mean ± SEM (A; n = 4 for each genotype).

ADAR1 competes with RIPK3 for ZBP1 binding to suppress inflammasome activation and cell death

Sensing of Z-RNA by the Zα domain of ZBP1 leads to the receptor-interacting protein homotypic interaction motif (RHIM) domain of ZBP1 interacting with the corresponding RHIM domain of RIPK3 to drive cell death (Devos et al., 2020; Jiao et al., 2020; Kesavardhana et al., 2020; Rebsamen et al., 2009). Because both ZBP1 and ADAR1 contain Zα domains, it is possible that ADAR1 interacts with ZBP1 via the Zα domains, thereby limiting the availability of ZBP1 for binding to RIPK3 and inhibiting the subsequent cell death.

We therefore sought to determine whether ZBP1 could interact with ADAR1 endogenously in WT BMDMs under different conditions. We observed that the expression of ADAR1 and ZBP1 was upregulated in response to IFN-β stimulation (Figure 6A). In addition, treatment with LMB was able to induce expression of ADAR1 and ZBP1, although the induction was not as robust as with IFN-β stimulation (Figure 6A). We also monitored the localization of ADAR1 and ZBP1 and found that treatment with the NEIs did not affect the localization of ZBP1 but did sequester ADAR1 in the nucleus (Figure S6A). In line with the low expression of ZBP1 and ADAR1 before IFN signaling activation, no interaction was observed between ZBP1 and ADAR1 under basal conditions (Figure 6B). However, we observed a robust interaction of ZBP1 with ADAR1, but not with RIPK3, in WT cells stimulated with IFN-β (Figure 6B). Although WT cells treated with KPT-330 or LMB alone showed some interaction of ZBP1 with both ADAR1 and RIPK3, stimulation with the combination of IFN-β with KPT-330 or LMB reduced the interaction of ZBP1 with ADAR1 and increased the interaction of ZBP1 with RIPK3 (Figure 6B). The increased interaction between ZBP1 and RIPK3 in response to IFNs and NEIs together compared with NEIs alone likely explains the increased cell death caused by this combination.

Because the homotypic interaction between ZBP1 and RIPK3 occurs via their RHIM domains (Rebsamen et al., 2009), we hypothesized that ZBP1 may interact with ADAR1 via their Zα domains. To determine whether the Zα domains of ZBP1 are critical for the interaction of ZBP1 with ADAR1, we generated hemagglutinin (HA)-tagged mutant ZBP1 constructs lacking Zα (ΔZα), RHIM (ΔRHIM), or C-terminal (Δ311–327) domains (Figure S6B) and overexpressed them in 293T cells. WT ZBP1 was co-immunoprecipitated with ADAR1 (Figure 6C). Although mutant forms of ZBP1 lacking the RHIM or C-terminal domains also co-immunoprecipitated with ADAR1, mutant ZBP1 lacking the Zα domains failed to efficiently pull down ADAR1 (Figure 6C). Similarly, ADAR1 co-immunoprecipitated with WT ZBP1 and the mutants lacking RHIM or C-terminal domains, but not the mutant lacking Zα domains (Figure 6C), indicating that ZBP1 interacts with

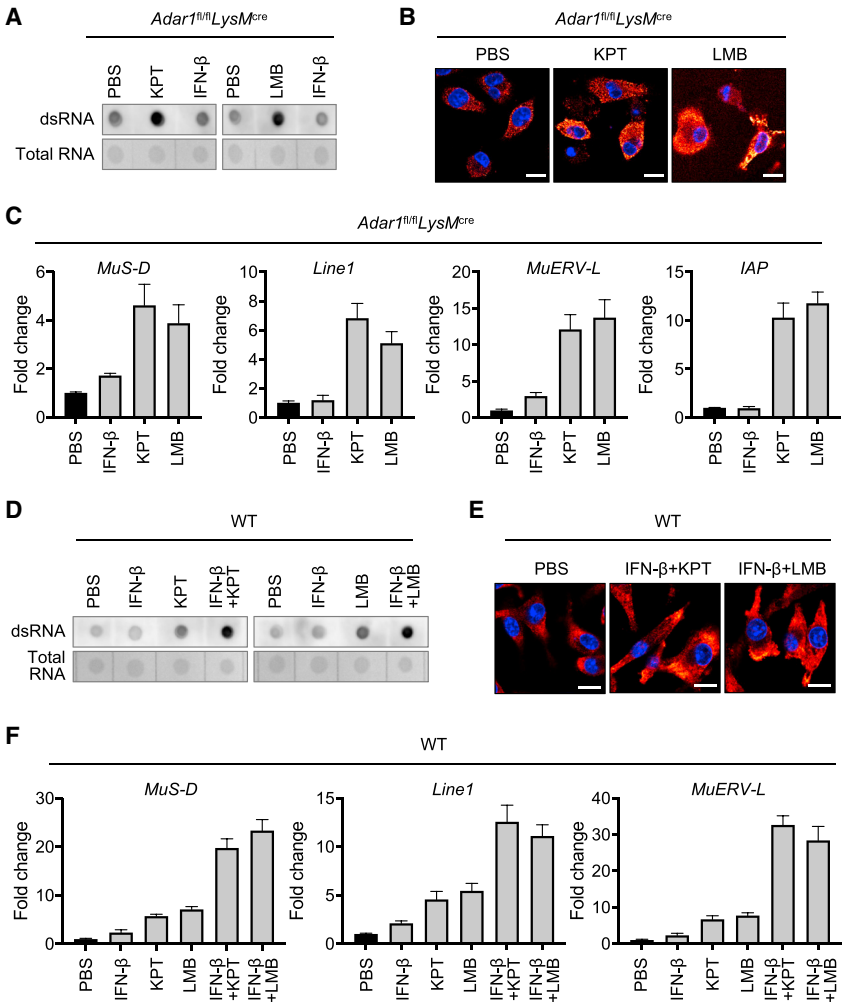

Figure 5. IFN signaling enhances the accumulation of double-stranded RNA (dsRNA) by nuclear export inhibitors

(A) Dot blot for dsRNA in *Adar1*$^{fl/fl}$*LysM*^{cre} BMDMs treated with KPT-330 (KPT), leptomycin B (LMB), or IFN-β for 8 h.

(B) Immunofluorescence staining of dsRNA (pseudocolored red hot in Fiji) and nucleus (blue) in *Adar1*$^{fl/fl}$*LysM*^{cre} BMDMs treated with KPT or LMB for 12 h.

(C) Expression analysis of endogenous retroelements *MuS-D*, *Line1*, *MuERV-L*, and *IAP* in *Adar1*$^{fl/fl}$*LysM*^{cre} BMDMs treated with KPT, LMB, or IFN-β for 8 h by real-time PCR.

(D) Dot blot for dsRNA in WT BMDMs treated with KPT, LMB, and/or IFN-β for 16 h.

(E) Immunofluorescence staining of dsRNA (pseudocolored red hot in Fiji) and nucleus (blue) in WT BMDMs treated with KPT or LMB in the presence of IFN-β for 24 h.

(F) Expression analysis of endogenous retroelements *MuS-D*, *Line1*, and *MuERV-L* in WT BMDMs treated with KPT, LMB, and/or IFN-β for 16 h by real-time PCR.

Data are representative of at least two independent experiments. Scale bars, 10 μm. Data are shown as mean ± SEM (C and F; n = 5 in each treatment group).

ADAR1 via its Zα domain. Among the two isoforms of ADAR1, only the p150 isoform contains the Zα domain and NES motif (Poulsen et al., 2001; Schwartz et al., 1999). However, we observed that ZBP1 interacted with both of the isoforms, p150 and p110 (Figures 6B and 6D). It is possible that these isoforms may exist as heterodimers and that the p110 isoform was pulled down while co-immunoprecipitating the p150 isoform with ZBP1 (Valente and Nishikura, 2007). Additionally, to further investigate this observation, we overexpressed the p150 and p110 isoforms of ADAR1 and determined their interaction with ZBP1. Cells overexpressing ADAR1-p150 showed a stronger interaction between ADAR1 and ZBP1 compared with cells overexpressing the p110 isoform (Figure S6C).

Although the importance of the interaction between ZBP1 and RIPK3 is well established in activating cell death pathways, the significance of the interaction between ZBP1 and ADAR1 that we identified in this study is not known. Because ADAR1 suppressed the ZBP1/RIPK3-mediated cell death, ADAR1 could potentially compete with RIPK3 for binding to ZBP1. To determine whether this occurs, we compared the endogenous interaction between ADAR1 and ZBP1 in the presence and absence of RIPK3, as well as the interaction between RIPK3 and ZBP1 in the presence and absence of ADAR1. We did not detect any interaction between ADAR1 and ZBP1 or RIPK3 and ZBP1 in WT BMDMs under basal conditions (Figure 6D). Upon treatment with IFN-β and KPT-330 or IFN-β and LMB, ZBP1 interacted with both ADAR1 and RIPK3 in WT BMDMs (Figures 6B and 6D). However, the interaction between ZBP1 and RIPK3 was increased in the absence of ADAR1 (Figures 6D and S6D). Furthermore, the interaction between ZBP1 and ADAR1 was increased in *Ripk3*$^{-/-}$ cells compared with that of WT cells (Figure 6D), suggesting that ADAR1 competes with RIPK3 for binding to ZBP1. Moreover, in the absence of its Zα2 domain, ZBP1 did not interact with RIPK3 in BMDMs treated with IFN-β and KPT-330 (Figure S6E), suggesting that the Zα2 domain of ZBP1 is required to facilitate the interaction between the RHIM domains of ZBP1 and RIPK3.

To further understand the mechanism through which the ADAR1-ZBP1 interaction was responsible for the cell death observed, we considered the potential role for PKR in this process. Previous studies have found that ADAR1 inhibits PKR (Clerzius et al., 2009; Li et al., 2010), and that PKR activation can be associated with cell death (Lee and Esteban, 1994; Yeung et al., 1996). To determine whether PKR was involved in the cell death observed here, we silenced PKR in BMDMs and treated them with the combination of IFN-β with KPT-330 or LMB; we observed no difference in the cell death (Figure S6F), suggesting that this is a PKR-independent mechanism.

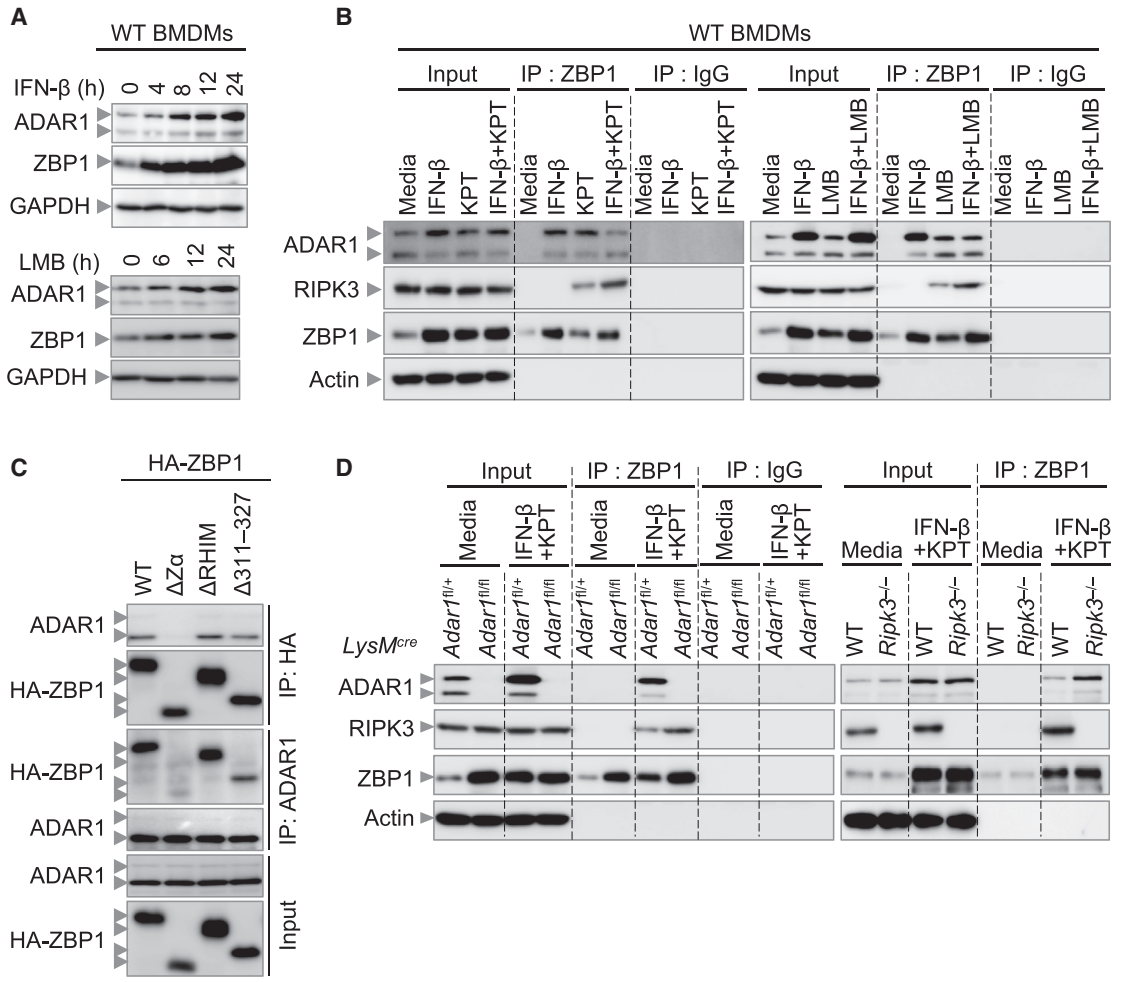

Figure 6. ADAR1 competes with RIPK3 for binding with ZBP1

(A) Immunoblot analysis of ADAR1 and ZBP1 in WT BMDMs stimulated with IFN-β or leptomycin B (LMB) for the indicated time.

(B) Immunoblot analysis of ADAR1, RIPK3, and ZBP1 following immunoprecipitation (IP) with anti-ZBP1 or IgG control antibodies in WT BMDMs 12 h after treatment with IFN-β, KPT-330 (KPT), LMB, IFN-β + KPT, or IFN-β + LMB.

(C) Immunoblot analysis of ADAR1 and HA-tagged ZBP1 following IP with anti-HA or anti-ADAR1 antibodies from lysates of 239T cells expressing HA-tagged ZBP1 constructs.

(D) Immunoblot analysis of ADAR1, RIPK3, and ZBP1 following IP with anti-ZBP1 or IgG control antibodies in *Adar1*$^{fl/+}$*LysM*^{cre} and *Adar1*$^{fl/fl}$*LysM*^{cre} BMDMs 8 h after and WT and *Ripk3*$^{-/-}$ BMDMs 12 h after treatment with IFN-β + KPT. GAPDH or actin was used as the internal control. Data are representative of at least three independent experiments.

Overall, our results show that ADAR1 interacts with ZBP1 via the ZBP1 Zα domain, and this interaction limits the availability of ZBP1 to bind with RIPK3 to activate PANoptosis.

ADAR1 promotes tumorigenesis by suppressing ZBP1-mediated inflammatory cell death

Dysregulated cell death and inflammatory responses are associated with tumorigenesis. Resistance to cell death, particularly apoptosis, is one of the founding hallmarks of cancer (Green and Evan, 2002; Hanahan and Weinberg, 2000, 2011) and can explain the failure of many existing anti-cancer therapies (Delbridge et al., 2012). Therefore, alternative mechanisms that drive multiple programmed cell death pathways simultaneously can be effective in eliminating cancer cells (Malireddi et al., 2021). Indeed, when apoptosis is not effective, alternative programmed cell death pathways pyroptosis or necroptosis and inflammasome activation are beneficial to eliminate cancer cells (Chefetz et al., 2019; Fu et al., 2013; Karki and Kanneganti, 2019; Karki et al., 2017; Lage et al., 2001; Nagarajan et al., 2019; Wang et al., 2017). Additionally, activation of PANoptosis has been shown to be beneficial in cancer treatment (Karki et al., 2020; Malireddi et al., 2021). However, certain host molecules may inhibit these pathways, promoting the development of cancers. Because ADAR1 inhibited inflammasome activation and cell death characterized by the activation of pyroptotic, apoptotic, and necroptotic effectors, we hypothesized that ADAR1 can promote tumorigenesis through this mechanism.

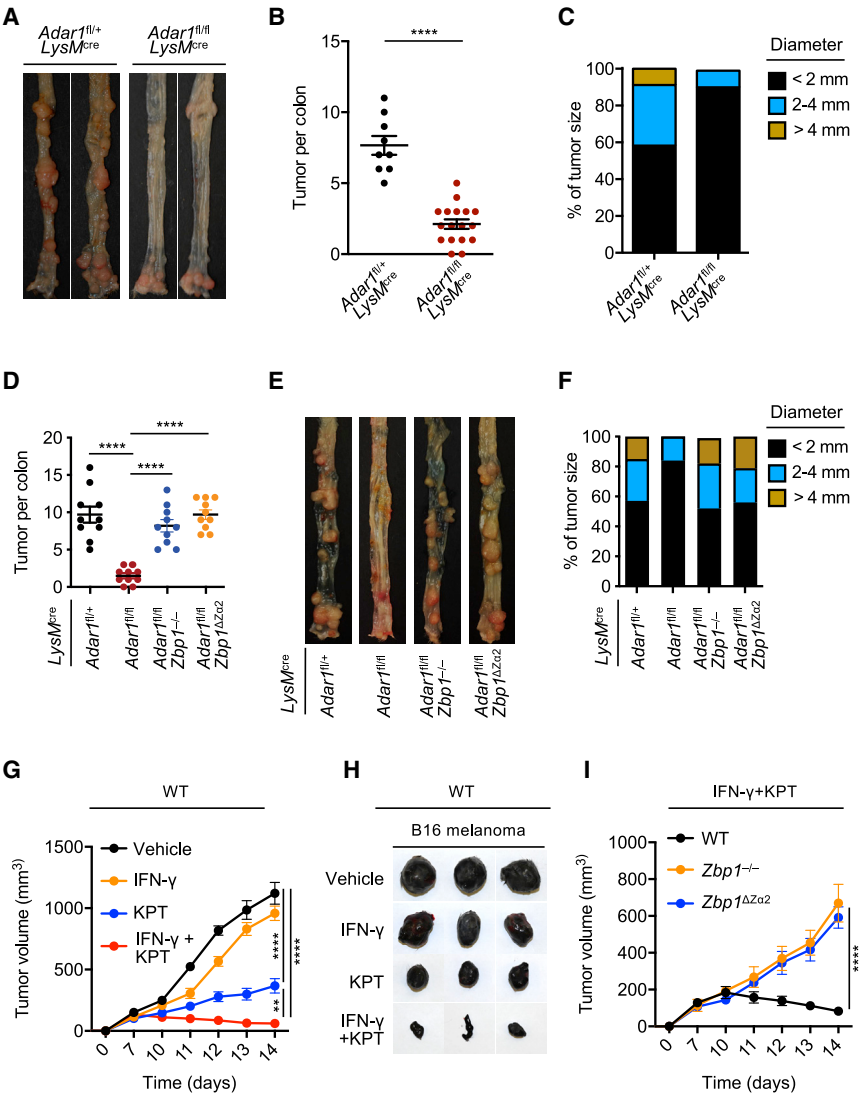

Figure 7. Modulation of the ADAR1-ZBP1 interaction affects tumorigenesis

(A) Representative images of colon tumors in *Adar1*$^{fl/+}$*LysM*^{cre} and *Adar1*$^{fl/fl}$*LysM*^{cre} mice 80 days after injection of azoxymethane (AOM).

(B) Number of colon tumors 80 days after AOM injection in *Adar1*$^{fl/+}$*LysM*^{cre} (n = 9) and *Adar1*$^{fl/fl}$*LysM*^{cre} (n = 17) mice.

(C) Percentage of tumors of various sizes 80 days after AOM injection in *Adar1*$^{fl/+}$*LysM*^{cre} (n = 9) and *Adar1*$^{fl/fl}$*LysM*^{cre} (n = 10) mice.

(D–F) Number of colon tumors (D); representative images of colon tumors (E); and percentage of tumors of various sizes (F) in *Adar1*$^{fl/+}$*LysM*^{cre} (n = 10), *Adar1*$^{fl/fl}$*LysM*^{cre} (n = 10), *Adar1*$^{fl/fl}$*LysM*^{cre}*Zbp1*$^{-/-}$ (n = 10), and *Adar1*$^{fl/fl}$*LysM*^{cre}*Zbp1*$^{\Delta Z\alpha 2}$ (n = 10) mice 80 days after AOM injection.

(G) Mean tumor volume in vehicle- (n = 10), IFN-γ- (n = 11), KPT-330- (KPT; n = 10), and IFN-γ + KPT-treated (n = 12) WT mice 2 weeks after B16-F10 melanoma cell engraftment. Mice were treated with IFN-γ and/or KPT on days 8, 10, and 13 after tumor engraftment.

(H) Representative tumor pictures from vehicle-, IFN-γ-, KPT-, and IFN-γ + KPT-treated WT mice.

(I) Mean tumor volume in IFN-γ + KPT-treated WT (n = 10), *Zbp1*$^{-/-}$ (n = 10), and *Zbp1*$^{\Delta Z\alpha 2}$ (n = 10) mice 2 weeks after injection of B16-F10 melanoma cells. Data are representative of at least three independent experiments. Each symbol represents one individual mouse (B and D).

**p < 0.01, ****p < 0.0001. Analysis was performed using the two-tailed t test (B) and the two-way ANOVA (D, G, and I). Data are shown as mean ± SEM (B, D, G, and I).

To investigate the role of ADAR1 and ADAR1-mediated cell death in tumorigenesis, we first determined the expression of *ADAR1* and *ZBP1* in several human cancer lines. All cancer cell lines from the NCI-60 panel showed high expression of *ADAR1* compared with that of *ZBP1* (Figure S7A), suggesting that ADAR1 and ZBP1 could differentially modulate tumorigenesis. To further understand the function of ADAR1 in tumor development, we used the established azoxymethane/dextran sodium sulfate (AOM/DSS) model of colorectal tumorigenesis in mice (Karki et al., 2016). The colons of *Adar1*$^{fl/fl}$*LysM*^{cre} mice had a lower tumor burden in terms of both number of tumors and tumor size compared with their littermate control mice (Figures 7A–7C). Histopathological analysis showed reduced thickening of the colons in *Adar1*$^{fl/fl}$*LysM*^{cre} mice compared with colons from the control mice (Figure S7B). Histological hallmarks associated with inflammation, ulceration, hyperplasia, and severity of damage were less frequently observed in the middle and distal colons of *Adar1*$^{fl/fl}$*LysM*^{cre} mice compared with the corresponding regions in the control mice (Figure S7C). To determine whether this suppression of tumorigenesis in *Adar1*$^{fl/fl}$*LysM*^{cre} mice was dependent on ZBP1, we subjected *Adar1*$^{fl/+}$*LysM*^{cre}, *Adar1*$^{fl/fl}$*LysM*^{cre}, and *Adar1*$^{fl/fl}$*LysM*^{cre}*Zbp1*$^{-/-}$ mice to AOM and DSS treatment. Although *Adar1*$^{fl/fl}$*LysM*^{cre} mice again showed a lower tumor burden, *Adar1*$^{fl/fl}$*LysM*^{cre}*Zbp1*$^{-/-}$ mice showed similar tumor burden with respect to the control mice (Figures 7D–7F). Furthermore, the deletion of the Zα2 domain of ZBP1 yielded similar results (Figures 7D–7F), suggesting that the ZBP1 Zα2 domain is crucial in suppressing colorectal tumorigenesis in mice lacking ADAR1 in myeloid cells. We further extended our analysis of the tumor-regulating function of ADAR1 and ZBP1 to melanoma. Mice were subcutaneously injected with melanoma cells and monitored for 2 weeks for tumor growth. We found that although *Adar1*$^{fl/fl}$*LysM*^{cre} mice exhibited significantly impaired tumor growth and lower tumor volume (Figure S7D), both *Zbp1*$^{-/-}$ and *Zbp1*$^{\Delta Z\alpha 2}$ mice developed larger melanoma tumors compared with control mice (Figure S7E). Furthermore, deletion of ZBP1 or the Zα2 domain of ZBP1 restored melanoma growth in *Adar1*$^{fl/fl}$*LysM*^{cre} mice to levels similar to that of control mice (Figure S7F). Together, these data suggest that ZBP1 is crucial in suppressing tumorigenesis in the absence of ADAR1.

In addition, we had observed that the inflammatory cell death induced by the combination of IFN and NEIs was dependent on

ZBP1 and mediated by changes in the interactions between ZBP1 and ADAR1 and RIPK3. Therefore, we sought to understand the efficacy of IFN and NEIs in treating melanoma. WT mice treated with KPT-330 8 days after B16 melanoma cell implantation showed reduced melanoma growth (Figures 7G and 7H). Moreover, mice treated with the combination of IFN-γ and KPT-330 had a significantly improved regression of their tumors (Figures 7G and 7H). To determine whether the tumor regression was dependent on ZBP1, we administered the combination of IFN-γ and KPT-330 to WT and *Zbp1*$^{-/-}$ mice. IFN-γ and KPT-330 failed to regress melanoma in the *Zbp1*$^{-/-}$ mice (Figure 7I). The deletion of the Zα2 domain of ZBP1 yielded similar results (Figure 7I), suggesting that ZBP1, as well as its Zα2 domain in particular, is crucial in suppressing tumorigenesis in response to treatment with the combination of IFN and NEIs.

DISCUSSION

In the current study, we observed contrasting roles in cell death for the only two mammalian proteins that contain Zα domains, ADAR1 and ZBP1. Whereas loss of ADAR1 led to increased inflammasome activation and cell death induced by IFNs and NEIs, loss of ZBP1 suppressed these processes. Mechanistically, we observed that the Zα2 domain of ZBP1 was required for its interaction with ADAR1. Moreover, ADAR1 competed with RIPK3 to associate with ZBP1 and modulate cell death. Similar competition resulting in contrasting roles for proteins in cell death has also been observed with the RHIM domain-containing proteins ZBP1 and RIPK1, where RIPK1 limits the binding of ZBP1 with RIPK3 to inhibit cell death (Lin et al., 2016; Newton et al., 2016). Additionally, the Zα domain of the E3 protein of vaccinia virus competes with ZBP1 for binding to Z-nucleic acids, thereby inhibiting ZBP1-RIPK3-mediated cell death (Koehler et al., 2017).

ADAR1 has important roles in homeostasis, and whole-body ADAR1 deficiency leads to embryonic lethality in mice, with MDA5 and PKR contributing to this lethality (Chung et al., 2018; Liddicoat et al., 2015; Pestal et al., 2015). However, mice lacking ADAR1 in myeloid cells are viable and developmentally normal, suggesting that ADAR1 is not essential in myeloid cells to maintain homeostasis. Although PKR and MDA5 contribute to lethality in ADAR1-deficient mice, our data show that PKR and MDA5 do not contribute to the cell death induced by IFNs and NEIs. Similarly, another study showed that deletion of *ADAR1* is not lethal to human embryonic stem cells, but that these cells exhibit spontaneous MDA5-mediated IFN-β production, PKR activation, and apoptosis upon differentiation to neural progenitor cells (Chung et al., 2018), indicating that requirements for ADAR1-mediated PKR or MDA5 inhibition depend on cell type and/or differentiation state. Instead, our data point to a critical interplay between ZBP1 and ADAR1 in regulating this cell death in macrophages. In ADAR1-deficient cells, the absence of RNA editing may allow endogenous dsRNAs to be stabilized and then recognized by the Zα domains of ZBP1 to activate inflammatory cell death, PANoptosis. Similarly, upon treatment with NEIs, ADAR1 is sequestered to the nucleus, which could compromise its RNA editing function. As a result, there could be an accumulation of dsRNA either in the presence of NEIs or in ADAR1-deficient cells that can lead to sensing by the innate immune system. Indeed, some ADAR1 substrates, such as transcripts from Alu elements, base pair to form duplex structures that are predicted to be destabilized by the ADAR1 editing to prevent their recognition by MDA5 and the subsequent induction of IFN production (Ahmad et al., 2018; Chung et al., 2018; Pfaller et al., 2018; Song et al., 2020), and dsRNA can accumulate following disruption of the Zα domain of ADAR1 to trigger MDA5-mediated IFN production (de Reuver et al., 2021). Our results show that ZBP1 is critically involved in the ADAR1-mediated modulation of cell death; therefore, it is also possible that the Zα domain of ADAR1 can sequester Z-RNAs to limit sensing by the Zα domains of ZBP1. We observed that treatment with NEIs led to the accumulation of dsRNA in the cell, and that this was potentiated by IFN signaling or loss of ADAR1. This suggests that the function of ADAR1 in the cytoplasm is important to prevent this dsRNA accumulation and subsequent cell death.

Although ADAR1 promotes tumorigenesis (Fumagalli et al., 2015; Han et al., 2015; Liu et al., 2019; Paz-Yaacov et al., 2015; Tassinari et al., 2021), its functions are protective against several autoinflammatory diseases through its regulation of IFN production and the subsequent IFN-mediated signaling (Lamers et al., 2019). ADAR1 safeguards neuronal cells from unwanted IFN production and cell death (Deng et al., 2020). Mutations in ADAR1 cause AGS (Rice et al., 2012), and our results suggest that the severe neuropathology associated with AGS may be explained by massive neuronal cell death mediated by overactivation of the ZBP1-RIPK3 axis in the absence of ADAR1. *Adar1* null mice succumb to embryonic lethality, as do mice with a specific deletion of ADAR1-p150, because of large amounts of cell death accompanied by an overproduction of type I IFNs and the resultant upregulation of ISGs, including ZBP1 (Hartner et al., 2004, 2009; Liddicoat et al., 2015; Wang et al., 2000). This perinatal lethality is rescued by the concurrent deletion of the RNA sensor MDA5 or the downstream adaptor protein mitochondrial antiviral signaling protein (MAVS) (Liddicoat et al., 2015; Pestal et al., 2015). However, deletion of MAVS or MDA5 fails to rescue the post-natal lethality caused by ADAR1 deficiency, indicating that there are MAVS signaling-independent developmental phenotypes in these mice (Liddicoat et al., 2015; Pestal et al., 2015). Indeed, we observed that loss of MAVS or MDA5 failed to prevent cell death induced by IFNs and NEIs, whereas loss of ZBP1 did prevent this cell death, indicating a potential role of ZBP1 in driving the lethality in the absence of ADAR1 in these mice.

In the context of cancer, our results indicate that increased expression of ADAR1-p150 limits ZBP1 binding to RIPK3, thereby inhibiting PANoptosis and allowing tumor growth. On the other hand, the absence of ADAR1 promoted ZBP1 binding to RIPK3, which mediated cell death and suppressed tumorigenesis and tumor growth. This paradigm is supported by the observation that there is a low level of expression of *ZBP1* in several human cancer lines. We also observed that the ADAR1-ZBP1 interaction can be pharmacologically modulated through combined treatment with IFN and NEIs. Using this combination in a melanoma model led to a significant reduction in tumor volume, suggesting that combining IFNs and NEIs, like the recently FDA-approved KPT-330, could be a potential strategy for clinical translation.

Historically, the success of IFN cancer therapies has been hindered by tumor resistance (Parker et al., 2016), possibly due to the induction of ADAR1-p150 and ZBP1 expression simultaneously by IFN. Indeed, immune modulators that increase IFN levels promote tumor resistance by inducing increased expression of ADAR1 in tumors (Ishizuka et al., 2019; Liu et al., 2019). NEIs specific to XPO1, such as KPT-330, cause ADAR1-p150 to accumulate in the nucleus, leading to cell death (Poulsen et al., 2001). Therefore, modulating the cytoplasmic localization of ADAR1-p150 using NEIs could increase the efficacy of IFN therapy during cancer treatment, consistent with our observation in the murine model. In addition to triggering ZBP1-mediated PANoptosis by sequestering ADAR1-p150 in the nucleus, KPT-330 treatment also leads to nuclear accumulation of a number of tumor suppressor genes, such as p53, causing cell-cycle arrest and apoptosis (Subhash et al., 2018). However, the regulation of p53-mediated cell death by ZBP1 and ADAR1 requires further investigation. In addition to its effects on IFN therapy, loss of function of ADAR1 improves responses to PD-1 blockade and overcomes common mechanisms of resistance to immunotherapy (Ishizuka et al., 2019). Collectively, this evidence suggests that targeting ADAR1 and the ADAR1-ZBP1 interaction represents a promising therapeutic strategy for future cancer treatments.

Overall, our findings show that ADAR1 functions as a checkpoint that limits anti-tumor immunity by suppressing ZBP1-mediated inflammatory cell death, PANoptosis, and suggest that strategies that affect the ADAR1-ZBP1 interaction, such as treatment with IFN and NEIs, could be therapeutically promising. These results provide deeper understanding of the cellular and molecular mechanisms of cell death, and specifically PANoptosis, and will be important to inform the development of effective treatment strategies against cancer.

Limitations and future directions

Our study defines the critical roles of ZBP1 and ADAR1 in mouse models of melanoma and colorectal carcinoma. Although our analysis of the expression of *ADAR1* and *ZBP1* in the NCI-60 human cancer lines supports that ADAR1 and ZBP1 could differentially modulate tumorigenesis in human cancers, additional work will be required to confirm the mechanistic interactions between ZBP1 and ADAR1 observed in this study are conserved in human cancers. Also, to fully understand the cell-intrinsic role of ZBP1 and ADAR1, future studies using ADAR1- and ZBP1-deficient B16-F10 melanoma cells are warranted. Furthermore, our study used murine BMDMs to decipher the combinatorial role of IFN and NEIs in inducing cell death and also found that this combination regressed tumors in a mouse model of melanoma significantly more than either individual therapy. Future studies to elucidate the role of this combination in inducing cell death in different cancer cell lineages will be important to further understand the potential to translate this into a therapeutic strategy for patients with cancer. Additionally, to understand the efficacy of this therapy in the clinical setting, it will be important to extend the evaluation of this therapy to humans. Therefore, initial safety assessments and, if safety signals are supportive, subsequent randomized controlled trials using these combinations in patients with cancer are critical to fully understand the potential application of this therapy in humans.

STAR★METHODS

Detailed methods are provided in the online version of this paper and include the following:

- KEY RESOURCES TABLE
- RESOURCE AVAILABILITY
  - Lead contact
  - Materials availability
  - Data and code availability
- EXPERIMENTAL MODEL AND SUBJECT DETAILS
  - Mice
  - Cell culture
- METHOD DETAILS
  - Cell stimulation
  - siRNA knockdown of PKR
  - Real-time imaging for cell death
  - Lactate dehydrogenase (LDH) assay for cell death
  - Isolation of cytosolic and nuclear fractions
  - Immunoblot analysis
  - Immunofluorescence staining
  - Co-immunoprecipitation assay
  - Microarray data analysis
  - RT-PCR analysis
  - AOM/DSS model of colorectal tumorigenesis
  - Histology and microscopy analysis
  - Melanoma model
- QUANTIFICATION AND STATISTICAL ANALYSIS

SUPPLEMENTAL INFORMATION

Supplemental information can be found online at https://doi.org/10.1016/j.celrep.2021.109858.

ACKNOWLEDGMENTS

We thank all the members of the Kanneganti laboratory for their comments and suggestions during the development of this manuscript. We also thank R. Tweedell, PhD, and J. Gullett, PhD, for scientific editing and writing support. Work from our laboratory is supported by the National Institutes of Health (AI101935, AI124346, AI160179, AR056296, and CA253095 to T.-D.K.) and the American Lebanese Syrian Associated Charities (to T.-D.K.). The content is solely the responsibility of the authors and does not necessarily represent the official views of the National Institutes of Health. We thank V.M. Dixit and N. Kayagaki (Genentech) for the *Casp11*$^{-/-}$ mutant mouse strain, and we thank Dr. Michael Gale for providing *Mavs*$^{-/-}$ mutant mice.

AUTHOR CONTRIBUTIONS

R.K. and T.-D.K. conceptualized the study; R.K. designed the methodology; R.K., B.S., B.R.S., S.L., R.K.S.M., L.N.N., M.Z., Y.W., and S.C. performed the experiments; P.S. and G.N. conducted the gene expression and publicly available dataset analysis; P.V. conducted the pathology analysis; R.K. and T.-D.K. wrote the manuscript with input from all the authors; T.-D.K. acquired the funding and provided overall supervision.

DECLARATION OF INTERESTS

St. Jude Children's Research hospital filed a provisional patent application on the IFN and NEI treatment strategy described in this study, listing R.K. and T.-D.K. as inventors (serial no. 63/196,986).

Received: March 9, 2021
Revised: August 12, 2021
Accepted: September 28, 2021
Published: October 19, 2021

REFERENCES

Ahmad, S., Mu, X., Yang, F., Greenwald, E., Park, J.W., Jacob, E., Zhang, C.Z., and Hur, S. (2018). Breaching self-tolerance to Alu duplex RNA underlies MDA5-mediated inflammation. Cell *172*, 797–810.e13.

Alexopoulou, L., Holt, A.C., Medzhitov, R., and Flavell, R.A. (2001). Recognition of double-stranded RNA and activation of NF-kappaB by Toll-like receptor 3. Nature *413*, 732–738.

Aricò, E., Castiello, L., Capone, I., Gabriele, L., and Belardelli, F. (2019). Type I interferons and cancer: An evolving story demanding novel clinical applications. Cancers (Basel) *11*, 1943.

Azizian, N.G., and Li, Y. (2020). XPO1-dependent nuclear export as a target for cancer therapy. J. Hematol. Oncol. *13*, 61.

Barrett, T., Wilhite, S.E., Ledoux, P., Evangelista, C., Kim, I.F., Tomashevsky, M., Marshall, K.A., Phillippy, K.H., Sherman, P.M., Holko, M., et al. (2013). NCBI GEO: archive for functional genomics data sets–update. Nucleic Acids Res. *41*, D991–D995.

Chari, A., Vogl, D.T., Gavriatopoulou, M., Nooka, A.K., Yee, A.J., Huff, C.A., Moreau, P., Dingli, D., Cole, C., Lonial, S., et al. (2019). Oral selinexor-dexamethasone for triple-class refractory multiple myeloma. N. Engl. J. Med. *381*, 727–738.

Chefetz, I., Grimley, E., Yang, K., Hong, L., Vinogradova, E.V., Suciu, R., Kovalenko, I., Karnak, D., Morgan, C.A., Chtcherbinine, M., et al. (2019). A pan-ALDH1A inhibitor induces necroptosis in ovarian cancer stem-like cells. Cell Rep. *26*, 3061–3075.e6.

Chen, K.W., Demarco, B., Heilig, R., Shkarina, K., Boettcher, A., Farady, C.J., Pelczar, P., and Broz, P. (2019). Extrinsic and intrinsic apoptosis activate pannexin-1 to drive NLRP3 inflammasome assembly. EMBO J. *38*, e101638.

Christgen, S., Zheng, M., Kesavardhana, S., Karki, R., Malireddi, R.K.S., Banoth, B., Place, D.E., Briard, B., Sharma, B.R., Tuladhar, S., et al. (2020). Identification of the PANoptosome: A molecular platform triggering pyroptosis, apoptosis, and necroptosis (PANoptosis). Front. Cell. Infect. Microbiol. *10*, 237.

Chung, H., Calis, J.J.A., Wu, X., Sun, T., Yu, Y., Sarbanes, S.L., Dao Thi, V.L., Shilvock, A.R., Hoffmann, H.H., Rosenberg, B.R., and Rice, C.M. (2018). Human ADAR1 prevents endogenous RNA from triggering translational shutdown. Cell *172*, 811–824.e14.

Clerzius, G., Gélinas, J.F., Daher, A., Bonnet, M., Meurs, E.F., and Gatignol, A. (2009). ADAR1 interacts with PKR during human immunodeficiency virus infection of lymphocytes and contributes to viral replication. J. Virol. *83*, 10119–10128.

de Reuver, R., Dierick, E., Wiernicki, B., Staes, K., Seys, L., De Meester, E., Muyldermans, T., Botzki, A., Lambrecht, B.N., Van Nieuwerburgh, F., et al. (2021). ADAR1 interaction with Z-RNA promotes editing of endogenous double-stranded RNA and prevents MDA5-dependent immune activation. Cell Rep. *36*, 109500.

Delbridge, A.R., Valente, L.J., and Strasser, A. (2012). The role of the apoptotic machinery in tumor suppression. Cold Spring Harb. Perspect. Biol. *4*, a008789.

Deng, P., Khan, A., Jacobson, D., Sambrani, N., McGurk, L., Li, X., Jayasree, A., Hejatko, J., Shohat-Ophir, G., O'Connell, M.A., et al. (2020). Adar RNA editing-dependent and -independent effects are required for brain and innate immune functions in Drosophila. Nat. Commun. *11*, 1580.

Devos, M., Tanghe, G., Gilbert, B., Dierick, E., Verheirstraeten, M., Nemegeer, J., de Reuver, R., Lefebvre, S., De Munck, J., Rehwinkel, J., et al. (2020). Sensing of endogenous nucleic acids by ZBP1 induces keratinocyte necroptosis and skin inflammation. J. Exp. Med. *217*, e20191913.

Eckmann, C.R., Neunteufl, A., Pfaffstetter, L., and Jantsch, M.F. (2001). The human but not the Xenopus RNA-editing enzyme ADAR1 has an atypical nuclear localization signal and displays the characteristics of a shuttling protein. Mol. Biol. Cell *12*, 1911–1924.

Fu, Z., Deng, B., Liao, Y., Shan, L., Yin, F., Wang, Z., Zeng, H., Zuo, D., Hua, Y., and Cai, Z. (2013). The anti-tumor effect of shikonin on osteosarcoma by inducing RIP1 and RIP3 dependent necroptosis. BMC Cancer *13*, 580.

Fumagalli, D., Gacquer, D., Rothé, F., Lefort, A., Libert, F., Brown, D., Kheddoumi, N., Shlien, A., Konopka, T., Salgado, R., et al. (2015). Principles governing A-to-I RNA editing in the breast cancer transcriptome. Cell Rep. *13*, 277–289.

George, C.X., and Samuel, C.E. (1999a). Characterization of the 5′-flanking region of the human RNA-specific adenosine deaminase ADAR1 gene and identification of an interferon-inducible ADAR1 promoter. Gene *229*, 203–213.

George, C.X., and Samuel, C.E. (1999b). Human RNA-specific adenosine deaminase ADAR1 transcripts possess alternative exon 1 structures that initiate from different promoters, one constitutively active and the other interferon inducible. Proc. Natl. Acad. Sci. USA *96*, 4621–4626.

Gitlin, L., Barchet, W., Gilfillan, S., Cella, M., Beutler, B., Flavell, R.A., Diamond, M.S., and Colonna, M. (2006). Essential role of mda-5 in type I IFN responses to polyriboinosinic:polyribocytidylic acid and encephalomyocarditis picornavirus. Proc. Natl. Acad. Sci. USA *103*, 8459–8464.

Gravina, G.L., Senapedis, W., McCauley, D., Baloglu, E., Shacham, S., and Festuccia, C. (2014). Nucleo-cytoplasmic transport as a therapeutic target of cancer. J. Hematol. Oncol. *7*, 85.

Green, D.R., and Evan, G.I. (2002). A matter of life and death. Cancer Cell *1*, 19–30.

Gurung, P., Anand, P.K., Malireddi, R.K., Vande Walle, L., Van Opdenbosch, N., Dillon, C.P., Weinlich, R., Green, D.R., Lamkanfi, M., and Kanneganti, T.D. (2014). FADD and caspase-8 mediate priming and activation of the canonical and noncanonical Nlrp3 inflammasomes. J. Immunol. *192*, 1835–1846.

Han, L., Diao, L., Yu, S., Xu, X., Li, J., Zhang, R., Yang, Y., Werner, H.M.J., Eterovic, A.K., Yuan, Y., et al. (2015). The genomic landscape and clinical relevance of A-to-I RNA editing in human cancers. Cancer Cell *28*, 515–528.

Hanahan, D., and Weinberg, R.A. (2000). The hallmarks of cancer. Cell *100*, 57–70.

Hanahan, D., and Weinberg, R.A. (2011). Hallmarks of cancer: the next generation. Cell *144*, 646–674.

Hartner, J.C., Schmittwolf, C., Kispert, A., Müller, A.M., Higuchi, M., and Seeburg, P.H. (2004). Liver disintegration in the mouse embryo caused by deficiency in the RNA-editing enzyme ADAR1. J. Biol. Chem. *279*, 4894–4902.

Hartner, J.C., Walkley, C.R., Lu, J., and Orkin, S.H. (2009). ADAR1 is essential for the maintenance of hematopoiesis and suppression of interferon signaling. Nat. Immunol. *10*, 109–115.

He, W.T., Wan, H., Hu, L., Chen, P., Wang, X., Huang, Z., Yang, Z.H., Zhong, C.Q., and Han, J. (2015). Gasdermin D is an executor of pyroptosis and required for interleukin-1β secretion. Cell Res. *25*, 1285–1298.

Ishii, K.J., Kawagoe, T., Koyama, S., Matsui, K., Kumar, H., Kawai, T., Uematsu, S., Takeuchi, O., Takeshita, F., Coban, C., and Akira, S. (2008). TANK-binding kinase-1 delineates innate and adaptive immune responses to DNA vaccines. Nature *451*, 725–729.

Ishizuka, J.J., Manguso, R.T., Cheruiyot, C.K., Bi, K., Panda, A., Iracheta-Vellve, A., Miller, B.C., Du, P.P., Yates, K.B., Dubrot, J., et al. (2019). Loss of ADAR1 in tumours overcomes resistance to immune checkpoint blockade. Nature *565*, 43–48.

Jiao, H., Wachsmuth, L., Kumari, S., Schwarzer, R., Lin, J., Eren, R.O., Fisher, A., Lane, R., Young, G.R., Kassiotis, G., et al. (2020). Z-nucleic-acid sensing triggers ZBP1-dependent necroptosis and inflammation. Nature *580*, 391–395.

Jones, J.W., Kayagaki, N., Broz, P., Henry, T., Newton, K., O'Rourke, K., Chan, S., Dong, J., Qu, Y., Roose-Girma, M., et al. (2010). Absent in melanoma 2 is required for innate immune recognition of Francisella tularensis. Proc. Natl. Acad. Sci. USA *107*, 9771–9776.

Kanneganti, T.D., Ozören, N., Body-Malapel, M., Amer, A., Park, J.H., Franchi, L., Whitfield, J., Barchet, W., Colonna, M., Vandenabeele, P., et al. (2006).

Bacterial RNA and small antiviral compounds activate caspase-1 through cryopyrin/Nalp3. Nature *440*, 233–236.

Karki, R., and Kanneganti, T.D. (2019). Diverging inflammasome signals in tumorigenesis and potential targeting. Nat. Rev. Cancer *19*, 197–214.

Karki, R., Lee, E., Place, D., Samir, P., Mavuluri, J., Sharma, B.R., Balakrishnan, A., Malireddi, R.K.S., Geiger, R., Zhu, Q., et al. (2018). IRF8 regulates transcription of Naips for NLRC4 inflammasome activation. Cell *173*, 920–933.e13.

Karki, R., Man, S.M., and Kanneganti, T.D. (2017). Inflammasomes and cancer. Cancer Immunol. Res. *5*, 94–99.

Karki, R., Man, S.M., Malireddi, R.K.S., Gurung, P., Vogel, P., Lamkanfi, M., and Kanneganti, T.D. (2015). Concerted activation of the AIM2 and NLRP3 inflammasomes orchestrates host protection against *Aspergillus* infection. Cell Host Microbe *17*, 357–368.

Karki, R., Man, S.M., Malireddi, R.K.S., Kesavardhana, S., Zhu, Q., Burton, A.R., Sharma, B.R., Qi, X., Pelletier, S., Vogel, P., et al. (2016). NLRC3 is an inhibitory sensor of PI3K-mTOR pathways in cancer. Nature *540*, 583–587.

Karki, R., Sharma, B.R., Lee, E., Banoth, B., Malireddi, R.K.S., Samir, P., Tuladhar, S., Mummareddy, H., Burton, A.R., Vogel, P., and Kanneganti, T.D. (2020). Interferon regulatory factor 1 regulates PANoptosis to prevent colorectal cancer. JCI Insight *5*, e136720.

Kayagaki, N., Warming, S., Lamkanfi, M., Vande Walle, L., Louie, S., Dong, J., Newton, K., Qu, Y., Liu, J., Heldens, S., et al. (2011). Non-canonical inflammasome activation targets caspase-11. Nature *479*, 117–121.

Karki, R., Sharma, B.R., Tuladhar, S., Williams, E.P., Zalduondo, L., Samir, P., Zheng, M., Sundaram, B., Banoth, B., Malireddi, R.K.S., et al. (2021). Synergism of TNF-α and IFN-γ triggers inflammatory cell death, tissue damage, and mortality in SARS-CoV-2 infection and cytokine shock syndromes. Cell *184*, 149–168.e17.

Kayagaki, N., Stowe, I.B., Lee, B.L., O'Rourke, K., Anderson, K., Warming, S., Cuellar, T., Haley, B., Roose-Girma, M., Phung, Q.T., et al. (2015). Caspase-11 cleaves gasdermin D for non-canonical inflammasome signalling. Nature *526*, 666–671.

Kesavardhana, S., Malireddi, R.K.S., Burton, A.R., Porter, S.N., Vogel, P., Pruett-Miller, S.M., and Kanneganti, T.D. (2020). The Zα2 domain of ZBP1 is a molecular switch regulating influenza-induced PANoptosis and perinatal lethality during development. J. Biol. Chem. *295*, 8325–8330.

Kim, D.D., Kim, T.T., Walsh, T., Kobayashi, Y., Matise, T.C., Buyske, S., and Gabriel, A. (2004). Widespread RNA editing of embedded alu elements in the human transcriptome. Genome Res. *14*, 1719–1725.

Koehler, H., Cotsmire, S., Langland, J., Kibler, K.V., Kalman, D., Upton, J.W., Mocarski, E.S., and Jacobs, B.L. (2017). Inhibition of DAI-dependent necroptosis by the Z-DNA binding domain of the vaccinia virus innate immune evasion protein, E3. Proc. Natl. Acad. Sci. USA *114*, 11506–11511.

Kumar, H., Kawai, T., Kato, H., Sato, S., Takahashi, K., Coban, C., Yamamoto, M., Uematsu, S., Ishii, K.J., Takeuchi, O., and Akira, S. (2006). Essential role of IPS-1 in innate immune responses against RNA viruses. J. Exp. Med. *203*, 1795–1803.

Kuriakose, T., Man, S.M., Malireddi, R.K., Karki, R., Kesavardhana, S., Place, D.E., Neale, G., Vogel, P., and Kanneganti, T.D. (2016). ZBP1/DAI is an innate sensor of influenza virus triggering the NLRP3 inflammasome and programmed cell death pathways. Sci. Immunol. *1*, aag2045.

Kuriakose, T., Zheng, M., Neale, G., and Kanneganti, T.D. (2018). IRF1 Is a Transcriptional Regulator of ZBP1 Promoting NLRP3 Inflammasome Activation and Cell Death during Influenza Virus Infection. J. Immunol. *200*, 1489–1495.

Lage, H., Helmbach, H., Grottke, C., Dietel, M., and Schadendorf, D. (2001). DFNA5 (ICERE-1) contributes to acquired etoposide resistance in melanoma cells. FEBS Lett. *494*, 54–59.

Lakhani, S.A., Masud, A., Kuida, K., Porter, G.A., Jr., Booth, C.J., Mehal, W.Z., Inayat, I., and Flavell, R.A. (2006). Caspases 3 and 7: key mediators of mitochondrial events of apoptosis. Science *311*, 847–851.

Lamers, M.M., van den Hoogen, B.G., and Haagmans, B.L. (2019). ADAR1: "Editor-in-chief" of cytoplasmic innate immunity. Front. Immunol. *10*, 1763.

Lee, S.B., and Esteban, M. (1994). The interferon-induced double-stranded RNA-activated protein kinase induces apoptosis. Virology *199*, 491–496.

Lee, S., Karki, R., Wang, Y., Nguyen, L.N., Kalathur, R.C., and Kanneganti, T.D. (2021). AIM2 forms a complex with pyrin and ZBP1 to drive PANoptosis and host defence. Nature *597* (*7876*), 415–419.

Li, Z., Wolff, K.C., and Samuel, C.E. (2010). RNA adenosine deaminase ADAR1 deficiency leads to increased activation of protein kinase PKR and reduced vesicular stomatitis virus growth following interferon treatment. Virology *396*, 316–322.

Liddicoat, B.J., Piskol, R., Chalk, A.M., Ramaswami, G., Higuchi, M., Hartner, J.C., Li, J.B., Seeburg, P.H., and Walkley, C.R. (2015). RNA editing by ADAR1 prevents MDA5 sensing of endogenous dsRNA as nonself. Science *349*, 1115–1120.

Lin, J., Kumari, S., Kim, C., Van, T.M., Wachsmuth, L., Polykratis, A., and Pasparakis, M. (2016). RIPK1 counteracts ZBP1-mediated necroptosis to inhibit inflammation. Nature *540*, 124–128.

Liu, H., Golji, J., Brodeur, L.K., Chung, F.S., Chen, J.T., deBeaumont, R.S., Bullock, C.P., Jones, M.D., Kerr, G., Li, L., et al. (2019). Tumor-derived IFN triggers chronic pathway agonism and sensitivity to ADAR loss. Nat. Med. *25*, 95–102.

Man, S.M., Karki, R., Sasai, M., Place, D.E., Kesavardhana, S., Temirov, J., Frase, S., Zhu, Q., Malireddi, R.K.S., Kuriakose, T., et al. (2016). IRGB10 Liberates Bacterial Ligands for Sensing by the AIM2 and Caspase-11-NLRP3 Inflammasomes. Cell *167*, 382–396.e17.

Malireddi, R.K.S., Karki, R., Sundaram, B., Kancharana, B., Lee, S., Samir, P., and Kanneganti, T.D. (2021). Inflammatory cell death, PANoptosis, mediated by cytokines in diverse cancer lineages inhibits tumor growth. Immunohorizons *5*, 568–580.

Man, S.M., Karki, R., and Kanneganti, T.D. (2017). Molecular mechanisms and functions of pyroptosis, inflammatory caspases and inflammasomes in infectious diseases. Immunol. Rev. *277*, 61–75.

Mariathasan, S., Newton, K., Monack, D.M., Vucic, D., French, D.M., Lee, W.P., Roose-Girma, M., Erickson, S., and Dixit, V.M. (2004). Differential activation of the inflammasome by caspase-1 adaptors ASC and Ipaf. Nature *430*, 213–218.

Murphy, J.M., Czabotar, P.E., Hildebrand, J.M., Lucet, I.S., Zhang, J.G., Alvarez-Diaz, S., Lewis, R., Lalaoui, N., Metcalf, D., Webb, A.I., et al. (2013). The pseudokinase MLKL mediates necroptosis via a molecular switch mechanism. Immunity *39*, 443–453.

Mutka, S.C., Yang, W.Q., Dong, S.D., Ward, S.L., Craig, D.A., Timmermans, P.B., and Murli, S. (2009). Identification of nuclear export inhibitors with potent anticancer activity in vivo. Cancer Res. *69*, 510–517.

Nagarajan, K., Soundarapandian, K., Thorne, R.F., Li, D., and Li, D. (2019). Activation of pyroptotic cell death pathways in cancer: An alternative therapeutic approach. Transl. Oncol. *12*, 925–931.

Neeman, Y., Levanon, E.Y., Jantsch, M.F., and Eisenberg, E. (2006). RNA editing level in the mouse is determined by the genomic repeat repertoire. RNA *12*, 1802–1809.

Newton, K., Sun, X., and Dixit, V.M. (2004). Kinase RIP3 is dispensable for normal NF-kappa Bs, signaling by the B-cell and T-cell receptors, tumor necrosis factor receptor 1, and Toll-like receptors 2 and 4. Mol. Cell. Biol. *24*, 1464–1469.

Newton, K., Wickliffe, K.E., Maltzman, A., Dugger, D.L., Strasser, A., Pham, V.C., Lill, J.R., Roose-Girma, M., Warming, S., Solon, M., et al. (2016). RIPK1 inhibits ZBP1-driven necroptosis during development. Nature *540*, 129–133.

Nishikura, K. (2010). Functions and regulation of RNA editing by ADAR deaminases. Annu. Rev. Biochem. *79*, 321–349.

Oberst, A., Dillon, C.P., Weinlich, R., McCormick, L.L., Fitzgerald, P., Pop, C., Hakem, R., Salvesen, G.S., and Green, D.R. (2011). Catalytic activity of the

caspase-8-FLIP(L) complex inhibits RIPK3-dependent necrosis. Nature *471*, 363–367.

Ozören, N., Masumoto, J., Franchi, L., Kanneganti, T.D., Body-Malapel, M., Ertürk, I., Jagirdar, R., Zhu, L., Inohara, N., Bertin, J., et al. (2006). Distinct roles of TLR2 and the adaptor ASC in IL-1beta/IL-18 secretion in response to Listeria monocytogenes. J. Immunol. *176*, 4337–4342.

Parker, B.S., Rautela, J., and Hertzog, P.J. (2016). Antitumour actions of interferons: implications for cancer therapy. Nat. Rev. Cancer *16*, 131–144.

Patterson, J.B., and Samuel, C.E. (1995). Expression and regulation by interferon of a double-stranded-RNA-specific adenosine deaminase from human cells: evidence for two forms of the deaminase. Mol. Cell. Biol. *15*, 5376–5388.

Paz-Yaacov, N., Bazak, L., Buchumenski, I., Porath, H.T., Danan-Gotthold, M., Knisbacher, B.A., Eisenberg, E., and Levanon, E.Y. (2015). Elevated RNA editing activity Is a major contributor to transcriptomic diversity in tumors. Cell Rep. *13*, 267–276.

Pestal, K., Funk, C.C., Snyder, J.M., Price, N.D., Treuting, P.M., and Stetson, D.B. (2015). Isoforms of RNA-editing enzyme ADAR1 independently control nucleic acid sensor MDA5-driven autoimmunity and multi-organ development. Immunity *43*, 933–944.

Pfaller, C.K., Donohue, R.C., Nersisyan, S., Brodsky, L., and Cattaneo, R. (2018). Extensive editing of cellular and viral double-stranded RNA structures accounts for innate immunity suppression and the proviral activity of ADAR1p150. PLoS Biol. *16*, e2006577.

Poulsen, H., Nilsson, J., Damgaard, C.K., Egebjerg, J., and Kjems, J. (2001). CRM1 mediates the export of ADAR1 through a nuclear export signal within the Z-DNA binding domain. Mol. Cell. Biol. *21*, 7862–7871.

Rebsamen, M., Heinz, L.X., Meylan, E., Michallet, M.C., Schroder, K., Hofmann, K., Vazquez, J., Benedict, C.A., and Tschopp, J. (2009). DAI/ZBP1 recruits RIP1 and RIP3 through RIP homotypic interaction motifs to activate NF-kappaB. EMBO Rep. *10*, 916–922.

Rice, G.I., Kasher, P.R., Forte, G.M., Mannion, N.M., Greenwood, S.M., Szynkiewicz, M., Dickerson, J.E., Bhaskar, S.S., Zampini, M., Briggs, T.A., et al. (2012). Mutations in ADAR1 cause Aicardi-Goutières syndrome associated with a type I interferon signature. Nat. Genet. *44*, 1243–1248.

Sarhan, J., Liu, B.C., Muendlein, H.I., Weindel, C.G., Smirnova, I., Tang, A.Y., Ilyukha, V., Sorokin, M., Buzdin, A., Fitzgerald, K.A., and Poltorak, A. (2019). Constitutive interferon signaling maintains critical threshold of MLKL expression to license necroptosis. Cell Death Differ. *26*, 332–347.

Schwartz, T., Rould, M.A., Lowenhaupt, K., Herbert, A., and Rich, A. (1999). Crystal structure of the Zalpha domain of the human editing enzyme ADAR1 bound to left-handed Z-DNA. Science *284*, 1841–1845.

Schwartz, T., Behlke, J., Lowenhaupt, K., Heinemann, U., and Rich, A. (2001). Structure of the DLM-1-Z-DNA complex reveals a conserved family of Z-DNA-binding proteins. Nat. Struct. Biol. *8*, 761–765.

Shen, J., Xu, S., Zhou, H., Liu, H., Jiang, W., Hao, J., and Hu, Z. (2017). IL-1β induces apoptosis and autophagy via mitochondria pathway in human degenerative nucleus pulposus cells. Sci. Rep. *7*, 41067.

Sheng, W., LaFleur, M.W., Nguyen, T.H., Chen, S., Chakravarthy, A., Conway, J.R., Li, Y., Chen, H., Yang, H., Hsu, P.H., et al. (2018). LSD1 ablation stimulates anti-tumorIlmmunity and enables checkpoint blockade. Cell *174*, 549–563.e19.

Shi, J., Zhao, Y., Wang, K., Shi, X., Wang, Y., Huang, H., Zhuang, Y., Cai, T., Wang, F., and Shao, F. (2015). Cleavage of GSDMD by inflammatory caspases determines pyroptotic cell death. Nature *526*, 660–665.

Skarnes, W.C., Rosen, B., West, A.P., Koutsourakis, M., Bushell, W., Iyer, V., Mujica, A.O., Thomas, M., Harrow, J., Cox, T., et al. (2011). A conditional knockout resource for the genome-wide study of mouse gene function. Nature *474*, 337–342.

Song, Y., Yang, W., Fu, Q., Wu, L., Zhao, X., Zhang, Y., and Zhang, R. (2020). irCLASH reveals RNA substrates recognized by human ADARs. Nat. Struct. Mol. Biol. *27*, 351–362.

Subhash, V.V., Yeo, M.S., Wang, L., Tan, S.H., Wong, F.Y., Thuya, W.L., Tan, W.L., Peethala, P.C., Soe, M.Y., Tan, D.S.P., et al. (2018). Anti-tumor efficacy of Selinexor (KPT-330) in gastric cancer is dependent on nuclear accumulation of p53 tumor suppressor. Sci. Rep. *8*, 12248.

Suthar, M.S., Ma, D.Y., Thomas, S., Lund, J.M., Zhang, N., Daffis, S., Rudensky, A.Y., Bevan, M.J., Clark, E.A., Kaja, M.K., et al. (2010). IPS-1 is essential for the control of West Nile virus infection and immunity. PLoS Pathog. *6*, e1000757.

Taabazuing, C.Y., Okondo, M.C., and Bachovchin, D.A. (2017). Pyroptosis and apoptosis pathways engage in bidirectional crosstalk in monocytes and macrophages. Cell Chem. Biol. *24*, 507–514.e4.

Tang, Z.L., Wang, S., Tu, C., Wang, T., Ma, C.W., Liu, Y., Xiao, S.X., and Wang, X.P. (2018). Eight novel mutations of the ADAR1 gene in Chinese patients with dyschromatosis symmetrica hereditaria. Genet. Test. Mol. Biomarkers *22*, 104–108.

Tassinari, V., Cesarini, V., Tomaselli, S., Ianniello, Z., Silvestris, D.A., Ginistrelli, L.C., Martini, M., De Angelis, B., De Luca, G., Vitiani, L.R., et al. (2021). ADAR1 is a new target of METTL3 and plays a pro-oncogenic role in glioblastoma by an editing-independent mechanism. Genome Biol. *22*, 51.

Taylor, J., Sendino, M., Gorelick, A.N., Pastore, A., Chang, M.T., Penson, A.V., Gavrila, E.I., Stewart, C., Melnik, E.M., Herrejon Chavez, F., et al. (2019). Altered nuclear export signal recognition as a driver of oncogenesis. Cancer Discov. *9*, 1452–1467.

Theodoropoulos, N., Lancman, G., and Chari, A. (2020). Targeting nuclear export proteins in multiple myeloma therapy. Target. Oncol. *15*, 697–708.

Valente, L., and Nishikura, K. (2007). RNA binding-independent dimerization of adenosine deaminases acting on RNA and dominant negative effects of nonfunctional subunits on dimer functions. J. Biol. Chem. *282*, 16054–16061.

Van Gorp, H., Saavedra, P.H., de Vasconcelos, N.M., Van Opdenbosch, N., Vande Walle, L., Matusiak, M., Prencipe, G., Insalaco, A., Van Hauwermeiren, F., Demon, D., et al. (2016). Familial Mediterranean fever mutations lift the obligatory requirement for microtubules in Pyrin inflammasome activation. Proc. Natl. Acad. Sci. USA *113*, 14384–14389.

Wang, Q., Khillan, J., Gadue, P., and Nishikura, K. (2000). Requirement of the RNA editing deaminase ADAR1 gene for embryonic erythropoiesis. Science *290*, 1765–1768.

Wang, Y., Gao, W., Shi, X., Ding, J., Liu, W., He, H., Wang, K., and Shao, F. (2017). Chemotherapy drugs induce pyroptosis through caspase-3 cleavage of a gasdermin. Nature *547*, 99–103.

Wang, R., Li, H., Wu, J., Cai, Z.Y., Li, B., Ni, H., Qiu, X., Chen, H., Liu, W., Yang, Z.H., et al. (2020). Gut stem cell necroptosis by genome instability triggers bowel inflammation. Nature *580*, 386–390.

Yang, D., Liang, Y., Zhao, S., Ding, Y., Zhuang, Q., Shi, Q., Ai, T., Wu, S.Q., and Han, J. (2020). ZBP1 mediates interferon-induced necroptosis. Cell. Mol. Immunol. *17*, 356–368.

Yeung, M.C., Liu, J., and Lau, A.S. (1996). An essential role for the interferon-inducible, double-stranded RNA-activated protein kinase PKR in the tumor necrosis factor-induced apoptosis in U937 cells. Proc. Natl. Acad. Sci. USA *93*, 12451–12455.

Yoneyama, M., Kikuchi, M., Natsukawa, T., Shinobu, N., Imaizumi, T., Miyagishi, M., Taira, K., Akira, S., and Fujita, T. (2004). The RNA helicase RIG-I has an essential function in double-stranded RNA-induced innate antiviral responses. Nat. Immunol. *5*, 730–737.

Zhang, T., Yin, C., Boyd, D.F., Quarato, G., Ingram, J.P., Shubina, M., Ragan, K.B., Ishizuka, T., Crawford, J.C., Tummers, B., et al. (2020). Influenza virus Z-RNAs induce ZBP1-mediated necroptosis. Cell *180*, 1115–1129.e13.

Zheng, T.S., Hunot, S., Kuida, K., Momoi, T., Srinivasan, A., Nicholson, D.W., Lazebnik, Y., and Flavell, R.A. (2000). Deficiency in caspase-9 or caspase-3 induces compensatory caspase activation. Nat. Med. *6*, 1241–1247.

Zheng, M., Karki, R., Vogel, P., and Kanneganti, T.-D. (2020). Caspase-6 Is a key regulator of innate immunity, inflammasome activation, and host defense. Cell *181*, 674–687.e13.

STAR★METHODS

KEY RESOURCES TABLE

REAGENT or RESOURCE	SOURCE	IDENTIFIER
Antibodies		
anti-caspase-3	Cell Signaling Technology	Cat# 9662; RRID: AB_331439
anti-cleaved caspase-3	Cell Signaling Technology	Cat# 9661; RRID: AB_2341188
anti-caspase-7	Cell Signaling Technology	Cat# 9492; RRID: AB_2228313
anti-cleaved caspase-7	Cell Signaling Technology	Cat# 9491; RRID: AB_2068144
anti-caspase-8	AdipoGen	Cat# AG-20T-0138-C100; RRID: AB_2490519
anti-cleaved caspase-8	Cell Signaling Technology	Cat# 8592; RRID: AB_10891784
anti-caspase-11	Novus Biologicals	Cat# NB120-10454; RRID: AB_2259600
anti-GAPDH	Cell Signaling Technology	Cat# 5174; RRID: AB_10622025
anti-pMLKL	Cell Signaling Technology	Cat# 37333; RRID: AB_2799112
anti-MLKL	Abgent	Cat# AP14272b; RRID: AB_11134649
anti-GSDMD	Abcam	Cat# ab209845; RRID: AB_2783550
anti-GSDME	Abcam	Cat# ab215191; RRID: AB_2737000
anti-caspase-1	AdipoGen	Cat# AG-20B-0044; RRID: AB_2490253
anti-β-actin	Proteintech	Cat# 66009-1-IG; RRID: AB_2687938
HRP-conjugated secondary anti-rabbit	Jackson ImmunoResearch Laboratories	Cat# 111-035-047; RRID: AB_2337940
HRP-conjugated secondary anti-mouse	Jackson ImmunoResearch Laboratories	Cat# 315-035-047; RRID: AB_2340068
HRP-conjugated secondary anti-rat	Jackson ImmunoResearch Laboratories	Cat# 112-035-003; RRID: AB_2338128
anti-ADAR1	Santa Cruz Biotechnology	Cat# sc-73408; RRID: AB_2222767
anti-ZBP1	AdipoGen	Cat# AG-20B-0010; RRID: AB_2490191
anti-RIPK3	Cell Signaling Technology	Cat# 95702; RRID: AB_2721823
anti-pSTAT1	Cell Signaling Technology	Cat# 7649; RRID: AB_10950970
anti-tSTAT1	Cell Signaling Technology	Cat# 14994; RRID: AB_2737027
anti-pIRF3	Cell Signaling Technology	Cat# 4947; RRID: AB_823547
anti-GFP	Santa Cruz Biotechnology	Cat# sc-9996; RRID: AB_627695
anti-IgG1	Cell Signaling Technology	Cat# 5415; RRID: AB_10829607
anti-dsRNA	Scicons	Cat# 10010200; RRID: AB_2651015
anti-dsRNA	Millipore	Cat# MABE1134; RRID: AB_2819101
anti-lamin B	Abcam	Cat# ab16048; RRID: AB_10107828
anti-HA	Millipore	Cat# 05-904; RRID: AB_417380
anti-IFNAR1	Bio X Cell	Cat# BE0241; RRID: AB_2687723
anti-PKR	Santa Cruz	Cat# sc-6282; RRID: AB_628150
Alexa Fluor 647-conjugated antibody against mouse IgG	Invitrogen	Cat# A21235; RRID: AB_2535804
Alexa Fluor 568-conjugated antibody against mouse IgG	Invitrogen	Cat# A11031; RRID: AB_144696
Chemicals, peptides, and recombinant proteins		
IMDM	Thermo Fisher Scientific	Cat# 12440053
Fetal bovine serum	Biowest	Cat# S1620
Non-essential amino acids	Thermo Fisher Scientific	Cat# 11140-050
Penicillin and streptomycin	Thermo Fisher Scientific	Cat# 15070-063
DPBS	Thermo Fisher Scientific	Cat# 14190-250
IFN-γ	Peprotech	Cat# 315-05

(*Continued on next page*)

Continued

REAGENT or RESOURCE	SOURCE	IDENTIFIER
IFN-β	PBL Assay	Cat# 12400-1
IL-6	Peprotech	Cat# 212-16
IL-1β	R&D	Cat# 201-LB-025)
TNF-α	Peprotech	Cat# 315-01A
Propidium iodide	Life Technologies	Cat# P3566
Protease inhibitor	Roche	Cat# 11697498001
Phosphatase inhibitor	Roche	Cat# 04906837001
Forte western HRP substrate	Millipore	Cat# WBLUF055
Methylene blue	Sigma	Cat# M9140
RNase A	Thermo Fisher Scientific	Cat# EN0531
Isoflurane	Piramal Critical Care	Cat# 66794-013-25
KPT-330	Selleckchem	Cat# S7252
Leptomycin B	Sigma	Cat# L2913
Normal goat serum	Life Technologies	Cat# 01-6201
SYBR Green	Applied Biosystems	Cat# 4368706
DAPI	Biotium	Cat# 40043
TRIzol	Thermo Fisher Scientific	Cat# 15596026
Azoxymethane	Millipore Sigma	Cat# A5486
Dextran sodium sulfate	Affymetrix	Cat# 9011-18-1
DMEM	Thermo Fisher Scientific	Cat# 11995-073
Pluronic F-68	GIBCO	Cat# 24040-032
Polyvinylpyrrolidone	Sigma	Cat# 81440
SMART siRNA pool, Eif2ak2	Dharmacon	Cat# M-040807-01-0005
siRNA buffer	Dharmacon	Cat# B-002000-UB-100
Critical commercial assays		
Affymetrix Whole Transcript Plus Expression Kit	Thermo Fisher Scientific	Cat# 902281
Affymetrix Clariom S Mouse Genechip Array	Thermo Fisher Scientific	Cat# 902930
High-Capacity cDNA Reverse Transcription Kit	Applied Biosystems	Cat# 4368814
LDH Assay Kit	Promega	Cat# G1780
NE-PER Nuclear and Cytoplasmic Extraction Reagents	Thermo Fisher Scientific	Cat# 78833
Deposited data		
ISG expression in *Adar1*$^{-/-}$ fibroblasts	Barrett et al., 2013; Liddicoat et al., 2015	GEO: GSE58917
BMDM microarray data	This paper	GEO: GSE184323
Expression in NCI-60 cancer cells	NCI-60 database	https://dtp.cancer.gov/discovery_development/nci-60/
Experimental models: Cell lines		
B16-F10	ATCC	Cat# CRL-6322; RRID: CVCL_0604
293T	ATCC	Cat# CRL-3216; RRID: CVCL_0063
Experimental models: Organisms/strains		
Ripk3$^{-/-}$ mice	Newton et al., 2004	N/A
Ripk3$^{-/-}$*Casp8*$^{-/-}$ mice	Oberst et al., 2011	N/A
Casp11$^{-/-}$ mice	Kayagaki et al., 2011	N/A
Adar1$^{fl/fl}$ mice	Hartner et al., 2004	Cat# 34620-JAX
Adar1$^{fl/fl}$*LysM*^{cre} mice	This paper	N/A

(*Continued on next page*)

Continued

REAGENT or RESOURCE	SOURCE	IDENTIFIER
Adar1$^{fl/fl}$*LysM*^{cre} *Zbp1*$^{-/-}$ mice	This paper	N/A
Adar1$^{fl/fl}$*LysM*^{cre} *Zbp* $^{\Delta Z\alpha 2}$ mice	This paper	N/A
Nlrp3$^{-/-}$ mice	Kanneganti et al., 2006	N/A
Nlrc4$^{-/-}$ mice	Mariathasan et al., 2004	N/A
Asc$^{-/-}$ mice	Özören et al., 2006	N/A
Aim2$^{-/-}$ mice	Jones et al., 2010	N/A
Nlrp3$^{-/-}$*Aim2*$^{-/-}$ mice	Karki et al., 2015	N/A
Casp1$^{-/-}$ mice	Man et al., 2016	N/A
Mefv$^{-/-}$ mice	Van Gorp et al., 2016	N/A
Casp3$^{-/-}$ mice	Zheng et al., 2000	N/A
Casp7$^{-/-}$ mice	Lakhani et al., 2006	N/A
Gsdmd$^{-/-}$ mice	Karki et al., 2018	N/A
Gsdme$^{-/-}$ mice	Skarnes et al., 2011	N/A
Mlkl$^{-/-}$ mice	Murphy et al., 2013	N/A
Gsdmd$^{-/-}$*Gsdme*$^{-/-}$	This paper	N/A
Gsdmd$^{-/-}$*Mlkl*$^{-/-}$	Christgen et al., 2020	N/A
Gsdmd$^{-/-}$*Gsdme*$^{-/-}$*Mlkl*$^{-/-}$	Karki et al., 2021	N/A
Tlr3$^{-/-}$ mice	Alexopoulou et al., 2001	N/A
Mda5$^{-/-}$ mice	Gitlin et al., 2006	N/A
Mavs$^{-/-}$ mice	Kumar et al., 2006; Suthar et al., 2010	N/A
Zbp1$^{-/-}$ mice	Ishii et al., 2008	N/A
Zbp1$^{\Delta Z\alpha 2}$ mice	Kesavardhana et al., 2020	N/A
Software and algorithms		
GraphPad Prism 8.0	GraphPad Software, Inc.	https://www.graphpad.com/
Affymetrix Expression Console v1.1	Thermo Fisher Scientific	https://www.thermofisher.com/us/en/home/life-science/microarray-analysis/microarray-analysis-instruments-software-services/microarray-analysis-software.html
Fiji	ImageJ	https://imagej.net/software/fiji/
DAVID	Laboratory of Human Retrovirology and Immunoinformatics	https://david.ncifcrf.gov
Ingenuity Pathways Analysis software	QIAGEN	https://digitalinsights.qiagen.com/products-overview/discovery-insights-portfolio/analysis-and-visualization/qiagen-ipa/
Gene Set Enrichment Analysis (GSEA)	The Broad Institute	https://www.gsea-msigdb.org/gsea/index.jsp

RESOURCE AVAILABILITY

Lead contact

Further information and requests for reagents may be directed to, and will be fulfilled by the lead contact Thirumala-Devi Kanneganti (thirumala-devi.kanneganti@stjude.org).

Materials availability

All unique reagents generated in this study are available from the Lead Contact.

Data and code availability

- The microarray data can be accessed in GEO under accession number GSE184323 and are publicly available as of the date of publication. Publicly available datasets were obtained from the NCI-60 database and from Barrett et al. (2013) and Liddicoat et al. (2015) (GEO: GSE58917). All other datasets generated or analyzed during this study are included in the published article. Microscopy data reported in this paper will be shared by the lead contact upon reasonable request.
- All software and packages applied are publicly available and listed in the key resources table. Key analysis parameters are described in the methods. This paper does not report original code.
- Any additional information required to reanalyze the data reported in this paper is available from the lead contact upon reasonable request.

EXPERIMENTAL MODEL AND SUBJECT DETAILS

Mice

Zbp1$^{-/-}$ (Ishii et al., 2008), *Zbp1*$^{\Delta Z\alpha 2}$ (Kesavardhana et al., 2020), *Ripk3*$^{-/-}$ (Newton et al., 2004), *Ripk3*$^{-/-}$*Casp8*$^{-/-}$ (Oberst et al., 2011), *Adar1*$^{fl/fl}$ (Hartner et al., 2004), *Nlrp3*$^{-/-}$ (Kanneganti et al., 2006), *Casp1*$^{-/-}$ (Man et al., 2016), *Mefv*$^{-/-}$ (Van Gorp et al., 2016), *Casp3*$^{-/-}$ (Zheng et al., 2000), *Casp7*$^{-/-}$ (Lakhani et al., 2006), *Gsdmd*$^{-/-}$ (Karki et al., 2018), *Gsdme*$^{-/-}$ (Skarnes et al., 2011), *Mlkl*$^{-/-}$ (Murphy et al., 2013), *Gsdmd*$^{-/-}$*Mlkl*$^{-/-}$ (Christgen et al., 2020), *Gsdmd*$^{-/-}$*Gsdme*$^{-/-}$*Mlkl*$^{-/-}$ (Karki et al., 2021), *Casp11*$^{-/-}$ (Kayagaki et al., 2011), *Asc*$^{-/-}$ (Ozören et al., 2006), *Tlr3*$^{-/-}$ (Alexopoulou et al., 2001), *Mavs*$^{-/-}$ (Kumar et al., 2006; Suthar et al., 2010), *Mda5*$^{-/-}$ (Gitlin et al., 2006), *Aim2*$^{-/-}$ (Jones et al., 2010), *Nlrp3*$^{-/-}$*Aim2*$^{-/-}$ (Karki et al., 2015), and *Nlrc4*$^{-/-}$ (Mariathasan et al., 2004) mice have been previously described. *Adar1*$^{fl/fl}$*LysM*^{cre}*Zbp1*$^{-/-}$ and *Adar1*$^{fl/fl}$*LysM*^{cre}*Zbp1*$^{\Delta Z\alpha 2}$ mice were bred by crossing *Adar1*$^{fl/fl}$*LysM*^{cre} and *Zbp1*$^{-/-}$ or *Zbp1*$^{\Delta Z\alpha 2}$ mice, respectively. *Gsdmd*$^{-/-}$*Gsdme*$^{-/-}$ and were bred by crossing *Gsdmd*$^{-/-}$ and *Gsdme*$^{-/-}$ mice. All mice were generated on or extensively backcrossed to the C57/BL6 background.

All mice were bred at the Animal Resources Center at St. Jude Children's Research Hospital and maintained under specific pathogen-free conditions. Both male and female mice were used in this study; age- and sex-matched 6- to 9-week old mice were used for *in vitro* and 7-to 8-week old mice were used for *in vivo* studies. Mice were maintained with a 12 h light/dark cycle and were fed standard chow. Animal studies were conducted under protocols approved by the St. Jude Children's Research Hospital committee on the Use and Care of Animals.

Cell culture

Primary mouse bone marrow-derived macrophages (BMDMs) were generated from the bone marrow of wild-type and the indicated mutant mice. Cells were grown for 5–6 days in IMDM (Thermo Fisher Scientific, 12440053) supplemented with 1% non-essential amino acids (Thermo Fisher Scientific, 11140-050), 10% FBS (Biowest, S1620), 30% L929 conditioned media, and 1% penicillin and streptomycin (Thermo Fisher Scientific, 15070-063). BMDMs were then seeded into the growth media at a concentration of 1×10^6 cells into 12-well plates and incubated overnight.

293T cells were cultured in DMEM (GIBCO, 11995-065) supplemented with 1% non-essential amino acids, 1% penicillin and streptomycin, and 10% FBS. The mouse melanoma cell line B16-F10 (ATCC® CRL-6322) was cultured in a humidified, 5% CO_2 incubator at 37°C, and grown in DMEM with 10% FBS and 100 U/mL penicillin/streptomycin.

METHOD DETAILS

Cell stimulation

BMDMs were treated with 5 μM of KPT-330 (Selleckchem, S7252) or 5 ng/mL of leptomycin B (Sigma, L2913) in the presence and absence of 50 ng/mL of IFN-γ (Peprotech, 315-05), 50 ng/mL of IFN-β (PBL Assay, 12400-1), 50 ng/mL of IL-6 (Peprotech, 212-16), 25 ng/mL of TNF-α (Peprotech, 315-01A), or 50 ng/mL of IL-1β (R&D, 201-LB-025) for 12, 16, or 24 h, as indicated. Wherever indicated, BMDMs were pre-treated with 10 μg/mL of anti-IFNAR1 (Bio X Cell, BE0241) antibody for 1 h followed by stimulation with KPT-330 or LMB in the presence or absence of IFN-β.

siRNA knockdown of PKR

The SMART siRNA pool for *Eif2ak2* (Dharmacon, M-040807-01-0005) was used to knockdown PKR in BMDMs. A total of 5 nmol was dissolved in 1X siRNA buffer (Dharmacon, B-002000-UB-100) at 100 μM, and 0.5 μL siRNA was added to 1×10^6 BMDMs. Electroporation was performed using the neon transfection system (Invitrogen), with parameters −1500 V, 1 pulse and 20-ms width. After electroporation, BMDMs were immediately transferred into 12-well plates with a seeding density of 1×10^6 cells per well. After 48 h of transfection, BMDMs were stimulated with NEIs along with IFN-β to assess cell death.

Real-time imaging for cell death

The kinetics of cell death were determined using the IncuCyte S3 (Essen BioScience) live-cell automated system. BMDMs (5×10^5 cells/well) were seeded in 24-well tissue culture plates. Cells were treated with the indicated stimuli and stained with propidium iodide (PI; Life Technologies, P3566) following the manufacturer's protocol. The plate was scanned, and fluorescent and phase-contrast images (4 image fields/well) were acquired in real-time every 1 h from 0 to 24 h post-treatment. PI-positive dead cells are marked with a red mask for visualization. The image analysis, masking, and quantification of dead cells were done using the software package supplied with the IncuCyte imager.

Lactate dehydrogenase (LDH) assay for cell death

Levels of lactate dehydrogenase released by cells were determined in the supernatant using the CytoTox 96 Non-Radioactive Cytotoxicity Assay (Promega, G1780) according to the manufacturer's instructions.

Isolation of cytosolic and nuclear fractions

The cytosolic and nuclear fractions of cells treated with KPT-330 or LMB for 12 h in the presence or absence of IFN-β were isolated using NE-PER Nuclear and Cytoplasmic Extraction Reagents (Thermo Fisher Scientific, 78833) according to the manufacturer's instructions.

Immunoblot analysis

Cell lysates and culture supernatants were combined in caspase lysis buffer (containing 1 × protease inhibitors [Roche, 11697498001], 1 × phosphatase inhibitors [Roche, 04906837001], 10% NP-40, and 25 mM DTT) and 4 × sample loading buffer (containing SDS and 2-mercaptoethanol) for immunoblot analysis of caspases. For immunoblot analysis of signaling components, supernatants were removed, and cells were washed once with DPBS (Thermo Fisher Scientific, 14190-250), followed by lysis in RIPA buffer and sample loading buffer. Proteins were separated by electrophoresis through 8%–12% polyacrylamide gels. Following electrophoretic transfer of proteins onto PVDF membranes (Millipore, IPVH00010), nonspecific binding was blocked by incubation with 5% skim milk, then membranes were incubated with primary antibodies against: caspase-3 (Cell Signaling Technology [CST], #9662, 1:1000), cleaved caspase-3 (CST, #9661, 1:1000), caspase-7 (CST, #9492, 1:1000), cleaved caspase-7 (CST, #9491, 1:1000), caspase-8 (AdipoGen, AG-20T-0138-C100, 1:1000), cleaved caspase-8 (CST, #8592, 1:1000), caspase-11 (Novus Biologicals, NB120-10454, 1:1000), caspase-1 (AdipoGen, AG-20B-0042, 1:1000), GAPDH (CST, #5174, 1:1000), ZBP1 (AdipoGen, AG-20B-0010, 1:1000), pMLKL (CST, #37333, 1:1000), tMLKL (Abgent, AP14272b, 1:1000), ADAR1 (Santa Cruz Biotechnology, sc-73408, 1:500), GSDMD (Abcam, ab209845, 1:1000), GSDME (Abcam, #19859, 1:1000), RIPK3 (CST, #95702, 1:1000), pSTAT1 (CST, #7649, 1:1000), tSTAT1 (CST, #14994, 1:1000), pIRF3 (CST, #4947, 1:1000), PKR (Santa Cruz, sc-6282, 1:1000), HA (Millipore, 05-904, 1:1000), GFP (Santa Cruz Biotechnology, sc-9996, 1:1000), lamin B (Abcam, ab16048, 1:500), and β-actin (Proteintech, 66009-1-IG, 1:1000). Membranes were then washed and incubated with the appropriate horseradish peroxidase (HRP)–conjugated secondary antibodies (Jackson ImmunoResearch Laboratories, anti-rabbit [111-035-047] 1:5000, anti-mouse [315-035-047] 1:5000, and anti-rat [112-035-003], 1:5000). Proteins were visualized using Immobilon Forte Western HRP Substrate (Millipore, WBLUF0500).

Dot blotting for dsRNA analysis was performed with total RNA isolated from the cells as previously described (Sheng et al., 2018). Equal volumes (2 μL containing 1 μg of RNA) of the RNA was dotted on Hybond N+ membrane (GE Healthcare, RPN203B), dried and autocrosslinked in a UV stratalinker 2400 (Stratagene, 5496A UV) two times. The membrane was then blocked in 5% milk in TBST for 1 h and probed with J2 antibody (Scicons, 10010200, 1:1000) at 4°C overnight. The membrane was then processed as described above. The total dsRNA was detected using 0.2% methylene blue (Sigma, M9140).

Immunofluorescence staining

BMDMs were washed with PBS and fixed in 4% paraformaldehyde for 15 min at room temperature, followed by permeabilization for 10 minutes in 0.5% Triton X-100. Cells were blocked in 5% normal goat serum (Life Technologies, 01-6201) for 1 h at room temperature. Samples were incubated with anti-ZBP1 antibody (Adipogen AG-20B-0010, 1:250) or anti-J2 (Millipore, MABE1134, 1:100) overnight at 4°C. Cells were then washed three times with PBS and incubated with Alexa Fluor 647-conjugated antibody against mouse immunoglobulin G (Invitrogen, A21235, 1:250) or Alexa Fluor 568-conjugated antibody against mouse immunoglobulin G (Invitrogen, A11031, 1:250) and counterstained with DAPI (Biotium, 40043) for 1 h at room temperature. Cells were washed three times with PBS and imaged using a Leica SP8 confocal microscope. dsRNA was pseudocolored red hot in Fiji for visualization.

Co-immunoprecipitation assay

BMDMs (10×10^6 cells) were seeded into 10-cm dishes and treated with IFN-β, KPT-330, LMB, IFN-β and KPT-330, or IFN-β and LMB for 12 h. Then, the cells were lysed in a buffer containing 20 mM Tris-HCl (pH 7.4), 100 mM NaCl, 30 mM KCl, and 0.1% NP-40. After centrifugation at 16,000 × g for 10 min, the lysates were incubated with anti-ZBP1 antibody (AdipoGen; AG-20B-0010) or IgG1 control antibody (CST, 5415) with protein A/G PLUS-Agarose (Santa Cruz Biotechnology) overnight at 4°C. After washing with the above buffer, the immunoprecipitated proteins were harvested by boiling in 1 × SDS loading buffer at 100°C for 5 min.

For the overexpression system, plasmids expressing HA-tagged ZBP1-WT, ΔZα, ΔRHIM, or Δ311-327 or GFP-tagged ADAR1-p110 or ADAR1-p150 and ZBP1 were transfected into 293T cells. After incubating for 48 h, cells were stimulated with IFN-β for

24 h. Then cells were lysed in NP-40 lysis buffer (0.1% NP-40, 150 mM NaCl, 50 mM HEPES), and 20 min later cell lysates were centrifuged at 13,000 rpm for 10 min. Supernatant was collected and incubated with 1.5 μg of the indicated primary antibody on a rocking platform at 4°C. After overnight incubation, protein A/G PLUS-Agarose beads were added and incubated for 2 h. Then the beads were collected by centrifugation after washing with lysis buffer 4 times. Finally, samples were harvested after boiling in 2 × SDS loading buffer at 100°C for 5 min.

Microarray data analysis

Transcripts were profiled for BMDMs obtained from *Adar1*$^{fl/+}$*LysM*^{cre} and *Adar1*$^{fl/fl}$*LysM*^{cre} mice. Total RNA (100 ng) was converted into biotin-labeled cDNA by using an Affymetrix Whole Transcript Plus Expression kit (Thermo Fisher Scientific, 902281) and was hybridized to an Affymetrix Clariom S Mouse Genechip Array (Thermo Fisher Scientific, 902930). After chips were stained and washed, array signals were normalized and transformed into $\log_2$ transcript expression values by using the robust multi-array average algorithm (Affymetrix Expression Console v1.1). Differential expression was defined by application of a threshold of FDR < 0.1 using the Cyber-T t test. Lists of differentially expressed transcripts were analyzed for 'functional enrichment' by using the DAVID bioinformatics database and Ingenuity Pathways Analysis software (QIAGEN). Pathways with altered activity levels were identified by using the Gene Set Enrichment Analysis (GSEA) with curated pathways obtained from The Broad Institute (http://software.broadinstitute.org/gsea/msigdb/).

Individual expression profiles (log2 signal) for *ADAR1* and *ZBP1* were extracted from the NCI-60 database. Publicly available transcriptomics data from fetal liver of WT and Adar1E861A (editing-deficient) mutant E12.5 embryos were obtained from Gene Expression Omnibus database (GEO: GSE58917) (Barrett et al., 2013; Liddicoat et al., 2015). Heatmap was generated from the 20 most upregulated ISGs.

RT-PCR analysis

Total RNA was extracted using TRIzol (Thermo Fisher Scientific, 15596026) and converted into cDNA by using the High-Capacity cDNA Reverse Transcription Kit (Applied Biosystems, 4368814). Real-time quantitative PCR was performed on an Applied Biosystems 7500 real-time PCR instrument with 2 × SYBR Green (Applied Biosystems, 4368706).

To determine the expression of EREs, 5 μg of total RNA extracted from the cells was dissolved in 46 μL of water and mixed well with 3.5 μL NaCl (5 M stock). Then, 0.5 μL RNase A (10 mg/mL stock, Thermo Fisher Scientific, EN0531) or water as mock was added to a total volume of 50 μL and mixed well, followed by incubation at room temperature for 10 min. Next, 1 mL TRIzol was directly added to the mixture to terminate digestion, followed by RNA extraction. The RNA transcripts of selected EREs were measure by RT-PCR with *Gapdh* as an internal control. The ratios of $(ERE/GAPDH)_{RNAase\text{-}A}/(ERE/GAPDH)_{mock}$ were calculated as enrichment folds (Sheng et al., 2018).

The sequences for qRT-PCR primers are listed in Table S1.

AOM/DSS model of colorectal tumorigenesis

Both male and female mice (littermate controls in experiments with *Adar1* mutants) were injected with 10 mg AOM (Millipore Sigma, A5486) per kg body weight according to previously established protocols (Karki et al., 2016). Five days later, 2.5% DSS (Affymetrix, 9011-18-1) was given in the drinking water for 6 days, followed by regular drinking water for 2 weeks. This DSS dosing cycle was repeated twice with 2% DSS, and mice were sacrificed on day 80. No randomization or blinding was performed.

Histology and microscopy analysis

Colons were rolled into a "Swiss roll" and fixed in 10% formalin and then processed and embedded in paraffin by standard techniques. Longitudinal sections of 5 μm thickness were stained with hematoxylin and eosin and examined by a pathologist blinded to the experimental groups. Histological scores were assigned based on inflammation, ulceration, hyperplasia, and the extent or severity of the damage. Severity scores for inflammation were assigned as follows: 0, normal (within normal limits); 2, minimal (mixed inflammation, small, focal, or widely separated, limited to lamina propria); 15, mild (multifocal mixed inflammation, often extending into submucosa); 40, moderate (large multifocal lesions within mixed inflammation involving mucosa and submucosa); 80, marked (extensive mixed inflammation with edema and erosions); and 100, severe (diffuse inflammation with transmural lesions and multiple ulcers). Scores for ulceration were assigned as follows: 0, normal (none); 2, minimal (only 1 small focus of ulceration involving fewer than 5 crypts); 15, mild (a few small ulcers, up to 5 crypts); 40, moderate (multifocal ulcers, up to 10 crypts); 80, marked (multifocal to coalescing ulcers involving more than 10 crypts each); and 100, severe (extensive to diffuse, with multiple ulcers covering more than 20 crypts each). Scores for hyperplasia were assigned as follows: 0, normal; 2, minimal (some areas with crypts elongated and increased mitoses); 15, mild (multifocal areas with crypts elongated up to twice the normal thickness, normal goblet cells present); 40, moderate (extensive areas with crypts up to 2 times normal thickness, reduced goblet cells); 80, marked (mucosa over twice the normal thickness, hyperchromatic epithelium, reduced or rare goblet cells, possibly foci of arborization); and 100, severe (mucosa twice the normal thickness, marked hyperchromasia, crowding/stacking, absence of goblet cells, high mitotic index, and arborization). Damage extent scores were assigned as follows: 0, normal (rare or inconspicuous lesions); 2, minimal (less than 5% involvement); 15, mild (multifocal but conspicuous lesions, 5%–10% involvement); 40, moderate (multifocal, prominent lesions, 10%–50%

involvement); 80, marked (coalescing to extensive lesions or areas of inflammation with some loss of structure, 50%–90% involvement); and 100, severe (diffuse lesion with effacement of normal structure, > 90% involvement).

Melanoma model

Male and female 6–12-week-old mice (littermate controls in experiments with *Adar1* mutants) were shaved on their lower back and engrafted with B16-F10 melanoma cells by subcutaneously injecting 1×10^6 cells in 200 μL PBS. Tumors were measured with digital calipers, and tumor volume was calculated using the formula: volume = (length × width^2) × ½. For treatment with IFN-γ (Peprotech, 315-05) each mouse was injected interperitoneally with 10 μg of IFN-γ in 100 μL of saline. For treatment with KPT-330 (Selleckchem, S7252), each mouse was administered orally with 300 μL of KPT-330 (15 mg/kg) suspended in 0.6% pluronic F-68 (GIBCO, 24040-032) and 0.6% polyvinylpyrrolidone (Sigma, 81440). Mice were randomly assigned to each treatment group. The treatment was given on days 8, 10, and 13 after tumor implantation.

QUANTIFICATION AND STATISTICAL ANALYSIS

GraphPad Prism 8.0 software was used for data analysis. Data are shown as mean ± SEM. Statistical significance was determined by t tests (two-tailed) for two groups or one-way ANOVA or two-way ANOVA for three or more groups. $p < 0.05$ was considered statistically significant.